Triassic alkaline magmatism of the Hawasina Nappes: Post-breakup melting of the Oman lithospheric mantle modified by the Permian Neotethyan Plume

François Chauvet, Henriette Lapierre, René Maury, Delphine Bosch, Christophe Basile, Joseph Cotten, Pierre Brunet, Sylvain Campillo

Triassic alkaline magmatism of the Hawasina Nappes: post-breakup melting of the Oman lithospheric mantle modified by the Permian Neotethyan Plume.

François Chauvet [a, b*], Henriette Lapierre [b†], René C. Maury [c], Delphine Bosch [d], Christophe Basile [b], Joseph Cotten [c], Pierre Brunet [e], Sylvain Campillo [b]

[a] *Université des Sciences de Nantes; CNRS-UMR 6112; Laboratoire de Planétologie et Géodynamique de Nantes, 2 rue de la Houssinière, BP 92208, 44322 Nantes Cedex 3, France.*

[b] *Université Joseph Fourier; CNRS-UMR 5025; Laboratoire de Géodynamique des Chaînes Alpines; Observatoire des Sciences de l'Univers de Grenoble, Maison des Géosciences 1381 rue de la Piscine, 38400 Saint Martin d'Hères, France.*

[c] *Université Européenne de Bretagne, Université de Brest; CNRS; UMR 6538 Domaines Océaniques; Institut Universitaire Européen de la Mer, Place N. Copernic, 29280 Plouzané, France.*

[d] *Université de Montpellier II; CNRS; UMR 5243 Géosciences Montpellier, Equipe Manteau-Noyau; Place E. Bataillon, 34095 Montpellier Cedex 05, France.*

[e] *Université Paul Sabatier; CNRS; UMR 5563 Laboratoire Mécanismes de Transfert en Géologie; Observatoire Midi-Pyrénées, 14 avenue E. Belin, 31400 Toulouse, France.*

* Corresponding author. Tel.: (33)251125474; fax: (33)251125268.

E-mail address: francois.chauvet@univ-nantes.fr

ABSTRACT

Middle to Late Triassic lavas were sampled within three tectonostratigraphic groups of the Hawasina Nappes in the Oman Mountains. They are predominantly alkali basalts and trachybasalts, associated with minor sub-alkaline basalts, trachyandesites, trachytes and rhyolites. Their major, trace elements and Nd-Pb isotopic compositions are very similar to those of the Permian plume-related high-Ti basalts which also occur in the Hawasina Nappes. The Triassic lavas derive from low-degree melting of an enriched OIB-type mantle source, characterized by εNd_i = 0.3-5.3 and $(^{206}Pb/^{204}Pb)_i$ = 16.96-19.31 (for t = 230 My). With time, melting depths decreased from the garnet + spinel to the spinel lherzolite facies and the degree of melting increased. The oldest are distinguished from the others by unradiogenic Nd and Pb signatures, with εNd_i = -4.5 to -1.2 and $(^{206}Pb/^{204}Pb)_i$ = 16.35-17.08, which we attribute to their contamination by Arabo-Nubian lower crust. The lavas likely derived from the Oman lithospheric mantle, the original DMM-HIMU signature of which was overprinted during its pervasive metasomatism by the Permian plume-related melts. We suggest that these lavas were emplaced during post-breakup decompression-triggered melting in the Middle Triassic during global kinematic reorganization of the Tethyan realm.

1. Introduction

Petrologic and geochemical studies of ancient oceanic crust and continental margins can be used to reconstruct the dynamics of past rifting and oceanization processes. The Middle Permian opening of the Neotethyan Ocean (Besse et al., 1998) separated Gondwana from Cimmerian continental blocks (Ricou, 1994; Stampfli and Borel, 2002). It led to the formation of passive continental margins south of the Neotethys Ocean, i.e. on the northern edges of the Australian, Indian, Arabian and African shields. Cretaceous to Neogene convergence between Laurasia and Gondwana (Stampfli and Borel, 2002) then led to the disappearance of Neotethyan oceanic crust. Fragments of its southern margins were incorporated into Alpine collisional belts in the Himalayas, Oman, Zagros, Syria, Cyprus, Turkey and Greece (Coleman, 1981, Fig. 1a).

These inverted margin fragments carry remnants of successive magmatic episodes, which can be used to constrain the formation and development stages of the southern Neotethyan margin. For instance, Middle Permian flood basalts are widespread in NW Indian (Panjal Traps) and Oman (Saih Hatat and Hawasina nappes Fig. 1a). Their plume-related geochemical features suggest that the breakup of Gondwana was associated with the emplacement of an intraplate volcanic province and associated volcanic-type margins (Garzanti et al., 1999; Maury et al., 2003; Lapierre et al., 2004; Chauvet et al., 2008). Younger (post-breakup) volcanic sequences are generally tectonically associated with Tethyan ophiolitic nappes, from the Himalayas to the eastern Mediterranean (Fig. 1a). Within these nappes, volcanic rocks are stratigraphically associated with late Middle to Late Triassic pelagic sediments and/or reef limestones. In the Oman Mountains, these Triassic post-breakup volcanic series have been considered as tectonically inverted intra-oceanic plateaus or seamounts (Glennie et al., 1974; Searle et al., 1980; Searle and Graham, 1982; Robertson and Searle, 1990; Stampfli et al., 1991; Pillevuit, 1993; Pillevuit et al., 1997), as well as their equivalents in the Himalayas (Ahmad et al., 1996; Robertson, 1998; Corfield et al. 1999) and Mediterranean sequences (Syria: Al Riyami and Robertson, 2002; Cyprus: Lapierre et al., 2007; Chan et al., 2008; Turkey: Maury et al., 2008; Greece: Monjoie et al., 2008),. Alternatively, the Oman Triassic lavas have been interpreted as remnants of a second rifting episode of the Arabian continental margin (Lippard et al., 1986; Béchennec et al., 1988, 1990, 1991).

A new petrologic and geochemical investigation (major and trace elements and Nd, Pb isotopes) of Middle to Late Triassic lavas from the allochthonous units of the Oman Mountains allows us to address these two hypotheses.

2. Geological setting

The Arabian continental margin of the Neotethys ocean formed during Permo-Triassic times (Béchennec et al., 1988; Robertson and Searle, 1990). Reconstructions of this margin (Glennie et al., 1974; Béchennec, 1987) suggest the occurrence of a continental platform (Saiq Fm.), a continental slope (Sumeini Group), and basinal environments (Hawasina units). In the Oman Mountains, remnants of several basins are exposed in the Hawasina Nappes, which are sandwiched between the autochthonous Arabian platform and the Semail ophiolitic nappe (Fig. 1b; Bernouilli and Weissert, 1987; Béchennec et al., 1988). They include Middle Permian (Murghabian) to Late Cretaceous sedimentary and volcanic units.

Béchennec (1987) and Béchennec et al. (1988, 1990, 1993) distinguished four tectonostratigraphic groups within the Hawasina Nappes tectonic pile (Fig. 1c,d). From the base to the top, they are the Hamrat Duru, Al Aridh, Kawr and Umar Groups (Fig. 1d). These groups were emplaced either in proximal (Hamrat Duru) or distal (Umar) pelagic basins, in a trench or slope (Al Aridh) or as an isolated carbonate platform (Kawr). While the Hamrat Duru basin appeared during the Middle Permian major rifting event, the three others (Al Aridh, Kawr and Umar Groups) formed during Middle to Late Triassic (de Wever et al., 1990). Because they are mainly found within tectonic slices, the remnants of the Hawasina Triassic carbonate platform were also named Oman Exotics (Glennie et al., 1974; Searle and Graham, 1982; Robertson and Searle, 1990) and the Umar Group volcanics correspond to the Haybi Volcanics of Searle et al. (1980). The latter authors performed geochemical analyses on a Permian and Triassic sample set coming from the northern part of the Oman Mountains.

Middle to Late Triassic volcanic sequences (ca. 10 to 100 m-thick) and associated magmatic intrusions occur (i) below and within the pelagic sediments of the Umar Group (Sinni Fm.); (ii) below and within the Kawr platform carbonates (Misfah Fm.); (iii) below the Al Aridh Group slope/trench deposits (Sayfam Fm.); and finally (iv) within the pelagic deposits of the Hamrat Duru Group (Matbat Fm.). Synsedimentary megabreccias intercalated within the proximal successions of the Hawasina Nappes (Watts, 1990; Pillevuit, 1993) suggest contemporaneous tectonic activity. This Middle to Late Triassic tectono-magmatic event occurred 30 to 40 My after the Middle Permian opening of Neotethys (Béchennec, 1987; Pillevuit, 1993; Baud et al., 2001).

3. Sampling and petrography

In this study, lavas from the Umar and Kawr Groups were sampled in the central part of the Oman Mountains, near the western termination of the Jabal Akhdar anticline (Al Qurti and Misfah localities, Fig. 1c,d). Additional samples were collected from three other Umar sites (Sinni, Sayjah and Aqil villages, Fig. 1c). The Al Aridh Group volcanics were sampled on the SW and NW flanks of the Jabal Buwaydah. Coeval volcanics from Hamrat Duru Group were not studied.

3.1. The Umar Group

The Umar Group is directly overthrusted by the Semail ophiolite (Fig. 1c,d). Its Triassic succession includes three lithofacies (UmV_{1-3}, Béchennec, 1987; Beurrier et al., 1986) which are well exposed as a succession of tectonic slices in the Al Qurti section (Appendix A). The 15 samples collected along this section exhibit the largest petrologic diversity of our suite, with, from base to top, basalts, trachyandesites, trachytes and rhyolites. The basal unit (UmV_1) corresponds to a 100 m thick succession of basaltic pillow-lavas, often tubular and dominated by subaphyric to porphyritic vesicular basalts with dispersed clinopyroxene phenocrysts (Om04-10, -11, -12). The second unit (UmV_2) includes basaltic flows capped with pelagic sediments (Om04-18, -19) and trachyandesitic pillowed lavas (Om04-17, -24, -27), successively overlain by hyaloclastites and volcanogenic debris flows. The latter contain rhyolitic lava blocks with plagioclase (Om04-29) and quartz grains (Om04-34, -35). The third unit (UmV_3), emplaced between the Kawr and Umar Groups, corresponds to columnar-jointed plugs showing trachytic textures with Na-rich plagioclase microcrysts and rare biotite phenocrysts (Om04-37, -38).

3.2. The Kawr Group

In the Hawasina nappes, the Kawr Group outcrops mainly south of the western termination of Jabal Akhdar anticline, in several mountains capped by high carbonate cliffs (Jabal Misht, Jabal Misfah, Jabal Kawr, and Jabal Ghul; Fig. 1c). Its stratigraphy (Béchennec, 1987; Pillevuit, 1993) has been defined on the northern and eastern slopes of Jabal Misfah (Appendix A). A 50 m thick basal volcanic unit, dated Ladinian-Carnian (Pillevuit, 1993) is made up of massive and pillowed basaltic flows, hyaloclastites and tuffites. These volcanics are successively overlain by Ladinian-Carnian to Rhaetian marly limestones, by thick and massive platform limestones crosscut by numerous basaltic dikes and sills, and finally by Jurassic to Cretaceous pelagic deposits. Among the 23 samples (Appendix A) collected from the Kawr Group, 11 come from the basal volcanic unit and 12 from the dykes and intrusive bodies. The basal flows, as well as the sills and dykes, show aphyric (Om04-52 and -54), microlitic (Om04-56, -59, -66), or highly porphyritic textures with abundant clinopyroxene phenocrysts (Om04-55, -57, -58).

3.3 The Al Aridh Group

The Al Aridh Group mainly outcrops along the southern flank of the Oman Mountains (Fig. 1c). It includes a basal volcanic sequence overlain by breccia horizons dated Middle/Late Triassic to Santonian (Béchennec et al., 1993). Seven samples were collected from two sites in Jabal Buwaydah, located south of the Jabal Kawr (Fig. 1c). The first one ("Buwaydah 1" in Fig. 1c) exposes a 40 m thick sequence of sills and massive flows, intercalated with basaltic pillows and overlain by a trachyandesitic flow. In the second locality ("Buwaydah 2" in Fig. 1c), the 150 m thick volcanic succession is capped by cherts and pelagic limestones dated Carnian to basal Norian (de Wever et al., 1990). The Al Aridh Group samples are porphyritic basaltic to trachyandesitic lavas with serpentinized olivine, fresh clinopyroxene and Fe-Ti oxides phenocrysts.

4. Geochemical data

4.1. Analytical methods

Sixty one samples (31 from the Umar, 23 from the Kawr and 7 from Al Aridh Group) were selected for petrographic and geochemical analysis. These rocks were pulverized in an agate mill and analysed using methods similar to those described in previous papers (see Chauvet et al., 2008 and references therein). Major elements and a set of trace elements (shown in italics in Table 1 and Appendix B) were determined by inductively coupled plasma-atomic emission spectrometry (ICP-AES) at the Université de Bretagne Occidentale in Brest, following the procedures of Cotten et al. (1995) and using international standards for calibration tests (AC-E, BE-N, JB-2, PM-S, WS-E). Rb contents were measured by flame atomic emission spectroscopy. Relative standard deviations were ~ 1 % for SiO_2 and 2 % for other major elements except P_2O_5 and MnO (0.01%), and ~ 5 % for trace elements. Additional trace element contents (Table 1) were measured by ICP-MS at the Université Joseph Fourier in Grenoble on 45 samples (27 from Umar, 14 from Kawr and 4 from Al Aridh), using the procedures of Barrat et al. (1996) and BHVO-2, BEN and BR-24 standards. Analytical errors were less than 3 % for trace elements except Cs (<5%).

Isotopic Nd and Pb data (Table 2) were corrected for *in situ* decay using an average age of 230 Ma (Ladinian-Carnian). All the Hawasina samples were leached twice in 6N HCl during 30 minutes at 100°C before acid digestion and Nd and Pb chemical separation in order to avoid or minimize alteration effects (see below). Nd (semi-dynamic acquisition) isotopic ratios of 21 samples labelled Om-29 to Om-207 were measured at LMTG, Université Paul Sabatier, Toulouse, on a Finnigan MAT 261 multicollector mass spectrometer using the analytical procedures of Lapierre et al. (1997). Results on standards yielded $^{143}Nd/^{144}Nd = 0.511958 \pm 34$ (n = 6) for the Neodymium Rennes Standard (Chauvel and Blichert-Toft, 2001). $^{143}Nd/^{144}Nd$ measured ratios were normalized for mass fractionation relative to $^{146}Nd/^{144}Nd = 0.7219$. In addition, 39 samples were selected for lead separation and leached with 6N tridistilled HCl during 30 minutes at 85°C before acid digestion (36-48 hours in ultrapure HF and HNO_3 acids). Pb blanks were less than 40 pg. Lead isotopes and Nd isotopic ratios of samples labelled "Om04-" and "Om05-" and Pb were measured on a Nu-plasma 500 multicollector magnetic-sector ICP-MS at the Ecole Normale Supérieure in Lyon. Details about chemical separations and isotope analytical measurements including reproducibility, accuracy and standards, can be found in Bosch et al. (2008) and references therein.

4.2. Alteration and sample selection

Ancient lavas are altered, a process that disturbs their major and trace element patterns and complicates calculation of initial isotopic ratios. Although our samples were carefully selected in the field, none of them is devoid of post-magmatic minerals and they often display numerous fractures filled with calcite, iron oxides and/or smectites. Pillow groundmass and vesicles contain variable amounts of calcite, zeolites and clays. In addition, the occasional presence of chlorite suggests that some Hawasina basin lavas underwent hydrothermal alteration or low-grade greenschist metamorphic conditions.

The loss on ignition (LOI) values of analyzed samples range from 2 to 13 wt.%, with more than half of them below 6 wt.% (Table 1 and Appendix B). Major elements analyses have been recalculated to 100% (volatile-free basis). The highest LOI values (> 10 wt.%) were measured in the Umar Group vesicular pillow lavas and in the Kawr Group intrusions, the groundmass of which is totally replaced by zeolites and calcite. Despite the high LOI values of the studied samples, SiO_2, MgO, Al_2O_3, P_2O_5 and TiO_2 contents variations from mafic to felsic lavas are relatively regular, and consistent with the petrographic (thin section) features of these rocks. In contrast, the large and erratic variations of CaO and Na_2O/K_2O at a given SiO_2 or MgO content (Table 1, Appendix B) or at a given "immobile" trace element content (e.g. Zr) suggests the mobility of alkaline and alkaline earth elements during alteration and/or recrystallization.

The analyzed samples display rather regular chondrite- and primitive mantle-normalized trace element patterns (Appendix C), with the exception of large ion lithophile elements (LILE). For instance, Rb, Ba and Sr exhibit strong negative or positive anomalies in multielement patterns which could have been generated either by their remobilization during post-magmatic processes (hydrothermalism and/or weathering) or by contamination processes during the evolution of their parental magmas. Nevertheless, the erratic behavior of Ca, Na, K and LILE is particularly obvious for samples showing the highest LOI and/or the largest amount of post-magmatic minerals. Thus, no attempt was made to use them to constrain igneous processes. In contrast, La, Nd, Sm, U and Pb correlate well with Th (Appendix D) and with high field strength elements (HFSE, not shown in Appendix D). These features suggest that the REE and HFSE contents of the studied samples, as well as their Pb and Nd isotopic compositions, represent reliable tools to investigate the petrogenesis of Hawasina Triassic lavas.

Sample selection for Pb isotopic analyses (39 samples out of the 54 analyzed for Nd, Appendix D) was aimed to eliminate the most altered samples and to account for the observed petrologic and geochemical variations. In the Pb and U *versus* Th diagrams (Appendix D), a majority of analyzed samples display Th/U and Th/Pb ratios close to the OIB mean values. However, despite a drastic sample selection, significant dispersions of Pb and U concentrations are still observed, particularly for Om-49 and Om-52 (Aqil), Om04-40 and -43 (Sayjah), Om04-12, -34 and -35 (Al Qurti). Related strong anomalies in multielement patterns and unusual ratios (Th/U < 2.5 and Th/Pb > 5) might indicate either post-magmatic alteration or open-system processes during magma ascent through the Arabian lithosphere.

4.3. Major elements and rock types

The analyzed lavas exhibit a wide range of SiO_2 (42 to 75 wt.%) and MgO contents (0.7 to 13 wt.%, Appendix B and Fig. 2a), even though mafic rocks (SiO_2 < 53 wt.% and MgO > 3 wt.%) are dominant. This chemical diversity is particularly obvious for the Umar samples which range from mafic to felsic (45-75 wt.% SiO_2, 11.1-0.7 wt.% MgO, Appendix B). Among mafic lavas characterized by SiO_2 < 53 wt.% and a basaltic-type petrographic assemblage in thin section, samples with MgO > 6 wt.% were classified as basalts (n = 26) and samples with 3 % < MgO < 6 wt.% as trachybasalts (n = 16). Both types have high P_2O_5 (0.18 < P_2O_5 < 1.58 wt.%) and high TiO_2 contents (1.5 < TiO_2 < 3.6 wt.%, Fig. 2b), with TiO_2 < 2 wt.% for only 7 out of 42 samples (Appendix B). These features are typical of alkaline magmas (Wilson, 1989). Despite the erratic behavior of alkali elements, a large majority of our sample set consistently plots within the alkaline field in the total alkali *versus* silica diagram (Fig. 2c). The very low Na_2O+K_2O values of Umar Si-rich lavas (Om04-29, -34 and 35) are probably linked to the widespread alteration of their groundmass.

4.4. Trace elements

Most Hawasina Triassic basalts and trachybasalts show enrichment in LREE and depletion in HREE and Y, features that are characteristic of intraplate magmas (Sun and McDonough, 1989; Willbold and Stracke, 2006). Their multielement patterns are very similar to OIB patterns (Fig. 3a,b), with enrichments culminating at Nb (Appendix C). When plotted in the Zr/Ti *versus* Nb/Y and Nb/Y *versus* Zr/Y diagrams (Fig. 4a,b), most of the samples yield Nb/Y ratios higher than 1, consistent with an alkaline affinity (Winchester and Floyd, 1977). In Fig. 4b, the studied mafic lavas plot within the field of alkali basalts from the Icelandic Neo-Volcanic Zone and away from the fields of Icelandic tholeiites and N-MORB (Fitton et al., 1997; Kokfelt et al., 2006).

The multielement diagrams of the Umar samples cluster into two main geochemical groups. The first (and by far the largest) one displays high enrichments in the most incompatible elements together with fractionated patterns ($La/Yb_N > 15$, Fig. 3a) and Nb/Y ratios higher than 1. This population hereafter referred to as the “alkali group”, includes all the samples from the UmV_1 basal unit of the Umar Group (Al Qurti section) and most UmV_2 lavas. The second group exhibits less fractionated patterns, with a lesser enrichment in the most incompatible elements and a more subdued depletion in the least incompatible elements ($5 < La/Yb_N < 15$, Fig. 3a, Appendix C). It includes a few lavas (Om-29, Om04-40, Om04-51, Om-42 and -52 from UmV_2 unit of the Umar Group) that display Nb/Y ratios lower than 1, together with rather low Zr/Ti ratios (Fig. 4a). As these features are consistent with either a mildly alkaline or even sub-alkaline (Om04-40) affinity, this group will be referred to as the “sub-alkaline group”.

4.5. Nd and Pb isotopes

4.5.1. Nd isotopic data

The initial Nd isotopic ratios of 54 analyzed samples range from 0.51211 to 0.51261 (i.e. εNd_i from +5.32 to -4.45; Table 2). The 44 positive εNd_i values are distributed among all the studied units, whereas the 10 negative εNd_i values are associated to the alkaline lavas of the Al Qurti UmV_1 (5 samples) and Sinni (5 samples) sections of the Umar Group (Table 2). εNd_i values of the 31 Umar samples cluster into three main groups characterized by (i) unradiogenic εNd_i values ($-4.5 < \varepsilon Nd_i < -1.2$), (ii) radiogenic εNd_i values ($2 < \varepsilon Nd_i < 4.4$), and (iii) intermediate εNd_i values, including two samples (Om04-40 and Om-97) with εNd_i of 0.52 and 0.34, respectively. The εNd_i of the latter two Umar groups encompass those of Kawr flows and Al Aridh lavas ($0.7 < \varepsilon Nd_i < 4.1$ and $1.2 < \varepsilon Nd_i < 3.2$), while Kawr intrusions yield more radiogenic Nd isotopic ratios with $3.1 < \varepsilon Nd_i < 5.3$ (Table 2).

4.5.2. Pb isotopic data

In Pb-Pb isotopic diagrams (Fig. 5a,b), Hawasina samples plot within an array subparallel to the Northern Hemisphere Reference Line (NHRL; Hart, 1984). Umar samples (n=23) exhibit highly variable Pb isotopic ratios, including both the most and the least radiogenic Pb compositions in our data set. They range from 16.35 to 19.31 for $(^{206}Pb/^{204}Pb)_i$, from 15.28 to 15.64 for $(^{207}Pb/^{204}Pb)_i$ and from 35.91 to 39.09 for $(^{208}Pb/^{204}Pb)_i$ (Table 2). Kawr and Al Aridh samples plot between these extremes. Kawr intrusions exhibit a wide range of Pb ratios which straddle that of the Kawr flows and Al Aridh samples. In the Pb-Pb correlation diagrams, the five samples that show the highest deviations from the main trend in Th-U and Th-Pb diagrams (Appendix C) generally plot within the OIB field, with the exception of the Om04-34 rhyolite which yields very unusual Pb ratios (Table 2). Such initial recalculated ratios could be linked to an overcorrection due to its particularly high Th contents compared to its low Pb concentration (Appendix B). Thus, this sample will not be considered in the following discussion.

4.5.3. Pb versus Nd isotopic ratios

With the exception of Kawr intrusions, which exhibit highly variable Pb isotopic ratios together with a restricted range of εNd_i values, the studied sample set shows a rough positive correlation in the εNd_i *versus* $(^{206}Pb/^{204}Pb)_i$ diagram (Fig. 5c). The observed scatter indicates that at least two isotopic end-members contributed to the geochemical signatures of the Hawasina Triassic magmatism (Fig. 5a,b,c).

5. Discussion

5.1. Fractionation, assimilation coupled with fractional crystallization and partial melting effects

The Umar UmV_2 trachyandesites, trachytes and rhyolites (Om04-17, -24, -27 and Om04-34 to -38) have negative Eu (and Ti) anomalies that are absent from UmV_1 and UmV_2 basaltic flows (Appendix C). The decrease of Al_2O_3 contents and Eu/Eu* ratios with increasing silica content (for $SiO_2 > 53$ wt.%, Fig. 6a,b) suggest that the Eu negative anomaly is correlated to plagioclase fractionation. However, a closed-system fractional crystallization process is not consistent with most REE variations. Indeed, UmV_2 basalts and trachyandesites (Om04-17 to 27) exhibit similar enrichments in La, but higher HREE and Y contents than UmV_1 basalts (Fig. 3a, Appendix C). Moreover, in Figure 6c, a jump in $(La/Yb)_N$ ratios is observed between UmV_1 basalts and UmV_2 lavas. The whole sample set displays positive correlations between La and $(La/Yb)_N$ (Fig. 6d), which are not consistent with closed-system fractionation.

The isotopic signatures of the studied lavas could be an intrinsic feature of their mantle source(s), or acquired *via* assimilation processes during magma ascent and/or storage within the Arabian lithosphere. Among our set, Umar samples exhibit the largest scatter of both SiO_2 contents and εNdi values. Their SiO_2 contents and trace elements ratios were plotted against εNdi values (Fig. 6e) to check the assimilation hypothesis. Umar alkali basalts seem to have preferentially sampled the Nd and Pb unradiogenic component. On the other hand, the silica-rich Umar lavas (UmV_2 trachyandesites, trachytes and rhyolites) exhibit εNd_i higher than those of basaltic lavas. Therefore, the relationships between the isotopic Nd signature and the silica contents of analyzed lavas are opposite to those expected for a shallow (upper) crustal assimilation process coupled with fractional crystallization (DePaolo, 1980), an increase of SiO_2 and a decrease in εNd_i.

The studied mafic lavas display $(La/Yb)_N$ variations dependant from variable La contents (Fig. 6d) and from significant variations of the HREE (trend 1 in Fig. 7a). A sample subset shows, in contrast, significant evolution of Yb contents (Fig. 7c) and $(Sm/Yb)_N$ ratios, without significant variations of La contents (trend 2 in Fig. 7a,b). As garnet has high distribution coefficients for HREE, $(La/Yb)_N$ and $(Sm/Yb)_N$ ratios are sensitive to the amount of residual garnet during partial melting (Caroff et al., 1997). An increasing melting degree of garnet-bearing lherzolite leads to a rapid decrease of La/Yb ratio without major Yb fractionation (Luhr et al., 1995). In contrast, increasing melting of spinel lherzolite will involve a more rapid Yb fractionation without significant variation of La/Yb ratio (Fig. 7c). In Figure 7c, Umar mafic lavas define two main trends delineated by the two grey domains. UmV_2 sub-alkaline basalts characterized by low $(La/Yb)_N$ ratios (< 10) show significant $(Sm/Yb)_N$ variations with highly variable Yb contents. They might derive from variable amounts of partial melting degrees (F ~ 5 to 10%) of a garnet-free lherzolitic source. In contrast, the older UmV_1 alkali basalts, which display high $(La/Yb)_N$ ratios (> 15) and low Yb contents (< 2 ppm) might derive from a lower amount (F ~ 3 to 6 %) of partial melting of a deeper (garnet+spinel-bearing) lherzolitic source. The Kawr and Al Aridh mafic lavas plot between the two Umar groups (Fig. 7c) and could have been generated at intermediate depths.

5.2. Evidence for source heterogeneity

The investigated mafic lavas display geochemical features similar to OIB and continental intraplate basalts, i.e. (i) incompatible element enrichments (Fig. 3) and (ii) Nd and Pb isotopic compositions clearly distinct from MORB (Fig. 5c). The most Nd- and Pb-radiogenic samples plot within the OIB field (Fig. 5), while the least Nd- and Pb-radiogenic ones (Umar alkali basalts) plot close to the Enriched Mantle 1 end-member (EM 1, Zindler and Hart, 1986; Fig. 5c). Their principal mantle source is distinct from the Depleted MORB Mantle

(DMM) in that the highest εNd_i value is +5.3 (Table 2). Moreover, the isotopic signatures of the Umar alkali basalts suggest a contribution of another source, one characterized by strongly enriched LREE patterns (Fig. 3a) relatively high La/Nb and Th/Nb ratios (Fig. 8a,b) and negative εNd_i signatures ($-4.5 < \varepsilon Nd_i < -1.2$) (Figs. 5c and 8).

In addition, the $(La/Sm)_N$ *versus* εNd_i plot (Fig. 8c) shows that the LREE enrichment of the basaltic samples is not coupled with Nd isotopic ratios. Indeed, it is greatest in the low εNd_i group (Umar basalts) and in the high εNd_i Kawr platform intrusions. In this diagram, the occurrence of two distinct isotopic groups and the lack of continuous trends suggest that the studied samples do not derive from the melting of variable mixes of two main mantle components. In that respect, they differ from most hotspot lavas which usually plot along linear trends connecting a depleted and an enriched mantle component in diagrams of Nd and Pb isotopic ratios and incompatible trace elements (Phipps Morgan and Morgan, 1999).

5.3. Possible geochemical imprint of the Arabian lithosphere

In the Ti/Y *versus* εNd_i plot (Fig. 8d), the studied basalts and trachybasalts show geochemical signatures characteristic of high-Ti continental flood basalts (Ti/Y>300-350; Hawkesworth et al., 1992; Gibson et al., 1995; Peate and Hawkesworth, 1996; Pik et al., 1998, 1999). Highly variable εNd_i values such as those observed for Hawasina lavas are often a characteristic of continental basalts. They are generally interpreted as markers of interactions between asthenosphere-derived melts and the local continental crust or the subcontinental lithospheric mantle (Saunders et al., 1992; Lightfoot et al, 1993; Sharma, 1997). As shown in Figs. 8a-b, the low εNd_i lavas from the Umar display a slight but significant depletion in Nb. This feature might be attributed to interactions with the local continental lithosphere, e.g. the lower crust or subcontinental lithospheric mantle.

The Arabo-Nubian shield includes oceanic terranes that formed and accreted during the Neoproterozoic Pan-African orogeny (Stern, 1994; Stein and Goldstein, 1996). These terranes are characterized by radiogenic Nd and Pb isotopic ratios ($+2 < \varepsilon Nd_i < +9$; Stoeser and Frost, 2006; Andersson et al., 2006). In addition, mafic and felsic granulites and peridotites, locally exhumed or found as xenoliths within Cenozoic lavas, sample of the Arabo-African lower continental crust and lithospheric mantle (Fig. 9). Their isotopic characteristics define a large domain of variation with, for instance, radiogenic Pb compositions ($^{206}Pb/^{204}Pb > 18$) and positive εNd_i signatures for Zabargad granulites and peridotites (Lancelot and Bosch, 1991; Hamelin and Allègre, 1988). Moreover, xenoliths from the Arabo-African lithospheric mantle also display radiogenic Nd ratios ($0.5135 < ^{143}Nd/^{144}Nd < 0.5129$), associated to $^{206}Pb/^{204}Pb >$ 17: these values are intermediate between DMM and high-μ (HIMU) end-members (Fig. 9). In addition, the predominant HIMU isotopic signature ($^{206}Pb/^{204}Pb$ = 18.60 to 19.55) of

Neogene-Quaternary intraplate basalts in Syria, Saudi Arabia and Yemen, has been interpreted as inherited from the Arabian lithospheric mantle (Bertrand et al., 2003).

The positive εNd of the Arabian lithospheric mantle (Fig. 9b) precludes it as the main source of the studied lavas, which have negative εNd values. Conversely, both the Nd and Pb isotopic ratios of the studied lavas plot within the compositional range of the Arabian upper and lower crusts. In particular, the isotopic compositions of alkali UmV_1 basalts match those of mafic granulites from the Yemen lower crust (Baker et al., 1997). This feature together with their slight Nb depletion suggests that the UmV_1 lavas signature might result from assimilation of lower crustal materials (Fig. 8a,b).

5.4. A Triassic Neotethyan plume beneath the Oman margin?

The OIB-like characteristics and predominantly alkali basaltic features of the Triassic Hawasina lavas have led many former authors (Glennie et al., 1974; Searle et al., 1980; Searle and Graham, 1982; Robertson and Searle, 1990; Stampfli et al., 1991; Pillevuit, 1993; Pillevuit et al., 1997) to consider them as hotspot-related intra-oceanic plateaus or seamounts. They might derive from either a genuine Triassic mantle plume or a still active Tethyan plume inherited from the Permian magmatic history. However, any isotopic (Figs. 5c and 10) or trace element (Fig. 4b) evidence for a depleted mantle component in their source is lacking. Conversely, Triassic depleted tholeiites occur in the Mamonia Complex, Cyprus (Lapierre et al., 2007), in Baër Bassit, Syria (Perez, 2006) and in Othrys, Greece (Monjoie et al., 2008). The isotopic signatures of Mediterranean Triassic volcanics (Fig. 10) are consistent with a mixing between the depleted upper mantle (main source of Mamonia, Baër Bassit and Othrys depleted tholeiites) and two mantle enriched components, HIMU and EM 2 (Perez, 2006; Lapierre et al., 2007; Maury et al., 2008). In contrast with the Oman case, none of these volcanics involved the contribution of lower crustal components with negative εNd_i to their genesis (Fig. 10). This feature suggests that they were emplaced on the Neotethyan oceanic floor rather than on a continental margin.

In addition, the hypothesis of a Triassic plume beneath the Oman margin does not fit available geological and chronological constraints. The preserved Triassic lava piles are less than 100 m thick, and thus very small with respect to plume-related magmatic successions such as traps, oceanic islands or rift-related series. The comparison of the Kawr platform with an intra-oceanic atoll built on the top of a seamount (Pillevuit, 1993; Pillevuit et al., 1997) has been invalidated by recent fieldwork (Basile and Chauvet, 2009). In addition, there is no evidence for magmatic activity in the Oman margin between the Permian (Wordian-Capitanian, ca. 265 Ma old) and the Middle-Late Triassic (Ladinian-Carnian, ca. 230 Ma old) events. This time gap is inconsistent with the hypothesis of survival of a Neotethyan plume since the Permian event.

5.5. An alternative hypothesis: melting of the Oman lithospheric mantle modified by the Permian plume.

Alkali basaltic magmas can be emplaced in regions removed from a mantle plume, providing that a distensional tectonic regime causes the uprise and partial melting of enriched lithospheric mantle (Wilson, 1989). Passage over an active mantle plume can indeed modify considerably the composition of the oceanic (Dupuy et al., 1993; Chauvel et al., 1997) or continental (Hawkesworth et al., 1990; Saunders et al., 1992; Lightfoot et al., 1993) lithospheric mantle, mainly through melt-induced metasomatism (Harry and Leeman, 1995; Downes, 2001). For instance, enriched pargasite-bearing mantle xenoliths from Morocco record the pervasive metasomatism of a depleted Proterozoic sublithospheric mantle by Tertiary plume-related HIMU-type alkaline melts which obliterated its initial composition (Raffone et al., 2009). The HIMU signature of Cenozoic alkali basalts from western Europe and their mantle xenoliths is attributed to mantle metasomatism of an heterogeneous lithospheric mantle by melts from an Early Tertiary asthenospheric plume (Hoernle et al., 1995; Downes, 2001). To test such a process, we have compared the compositions of the studied Triassic Hawasina lavas and those of their predecessors, i.e. the Permian Hawasina basalts which are clearly plume-related (Maury et al., 2003; Lapierre et al., 2004).

The Permian Hawasina basaltic piles include high-Ti alkali melts and low-Ti tholeiitic melts (Fig. 11a), the latter displaying low $(La/Sm)_N$ ratios (Fig. 11b) and either slightly enriched or slightly depleted multielement patterns (Fig. 11c). On the basis of Nd and Pb isotopic data, Lapierre et al. (2004) defined three different geochemical groups. Group 1 low-Ti tholeiitic basalts are characteristic of the most distal environments of the Hawasina Permian basin. They have variable but radiogenic Nd isotopic ratios ($3.8 < \varepsilon Ndi < 11.1$, Fig. 12a,b), together with rather homogeneous Pb isotopic ratios (Fig. 12c). Group 2 high-Ti alkali basalts are systematically associated with the proximal basin environments, and are more enriched in La, Th and Nb than Group 1 basalts (Fig. 11b,c). They are characterized by less radiogenic Nd isotopic ratios ($3.1 < \varepsilon Ndi < 4.9$; Fig. 12a,b). Finally, Group 3 includes high-Ti and low-Ti basalts (Fig. 11a) that erupted onto the continental platform of the Arabian margin, except for one basalt from the distal basin (top left of Fig. 11c). These Group 3 basalts are systematically enriched in the most incompatible trace elements and they have unradiogenic Nd isotopic ratios ($-2 < \varepsilon Ndi < 1.6$) and Pb isotopic ratios similar to those of Group 2 lavas (Fig. 12).

The trace element compositions of the Triassic Hawasina volcanics are overall very similar to those of Groups 2 and 3 high-Ti Permian basalts (Fig. 11c). Moreover, with the exception of Kawr intrusions and UmV_1 alkali basalts, the Nd and Pb isotopic compositions of Triassic Hawasina basalts match those of Groups 2 and 3 Permian basalts (Fig. 12). The UmV_1 basalts show Nd and Pb compositions less radiogenic than those of Group 3 lavas (Fig. 12c).

The above comparison shows that a component equivalent to that which generated the Permian Group 1 distal tholeiites has not been detected in the studied samples. Conversely, the Hawasina Triassic lavas are isotopically similar to Permian Groups 2 and 3 lavas, respectively (Fig. 12c). It is therefore possible to consider the OIB-type source of Permian Group 2 alkali basalts as identical or closely similar to the source of most Triassic volcanics (UmV_2 unit, Kawr intrusions and the majority of Al Aridh lavas). It might thus represent the main mantle reservoir underlying the Arabian margin since Middle Permian times (component A in Fig. 12a,b). The Kawr intrusions, which display higher La/Sm and La/Nd ratios than other Triassic lavas, could derive from low-degree melting of this source (trend B in Fig. 12a,b).

In the La/Nb, $(La/Sm)_N$ and La/Nd *versus* εNdi diagrams (Figs. 8a and 12a,b), Kawr basaltic flows plot between the main radiogenic and unradiogenic components. Trend C, drawn in $(La/Sm)_N$ and La/Nd *versus* εNdi plots, suggests that their source might be a mixture between OIB-type mantle (component A) and an enriched component. This trend has no equivalent among the Permian basalts, but the number of samples defining it is too limited for detailed interpretation.

Finally, the trend towards EM 1 (Fig. 12c) of Permian Group 3 and Triassic UmV_1 alkali basalts might result from their interaction with the lower crust (trend D in Fig. 12a,b). According to Lapierre et al. (2004), contamination of Group 3 Permian lavas would involve rocks similar in composition to the gneissic granulites of Zabargad Island. In contrast, UmV_1 basalts have Nd and Pb isotopic ratios that are lower than those of Zabargad granulites (Fig. 9), and more consistent with the composition of mafic lower crustal xenoliths (Baker et al., 1997).

In short, we propose that Permian plume-related alkaline melts metasomatized the Oman lithospheric mantle during their ascent towards the surface, overprinting its initial DMM-HIMU signature. Thirty-five million years later, a post-breakup extension induced partial melting of this metasomatized mantle, and generated the Triassic basaltic magmas. During their ascent, some of the oldest and deepest melts (UmV_1 basalts) interacted with rocks from the lower continental crust.

5.6. Tectonic framework of the Triassic volcanic event

Coeval (Ladinian – Carnian) volcanic sequences were emplaced all along the southern Tethyan realm. They were interpreted either as belonging to the southern Neotethyan continental margin series (e.g. Béchennec et al., 1988, 1991) or alternatively as oceanic island on the Neotethyan oceanic floor (Stampfli et al. 1991; Pillevuit et al., 1997). The lower crustal contamination suffered by the oldest Triassic basalts in the Umar basin (UmV_1) indicates that distal parts of the Hawasina basin overlay continental crust during the Triassic. The concomitant synsedimentary destabilizations of its continental slope and basin environments (Watts, 1990; Pillevuit, 1993) suggest a link between the Triassic magmatic event and extensional (post-breakup) tectonic reactivation of the Permian structures.

The Neotethys opened between the northern edge of Gondwana and the Cimmerian continental blocks. These blocks drifted northward during the subduction of the Paleotethys beneath the Southern Laurasia active margin (Besse et al., 1998). At the end of the Middle Triassic (Anisian), Paleotethyan subduction ended and was replaced by that of the Neotethys (Saidi et al., 1997; Besse et al., 1998). In geodynamic reconstructions, this subduction jump is generally linked to a global kinematic reorganization of the Tethyan realm. It is either attributed to a Neotethys ridge jump (Dercourt et al., 1993; Besse et al., 1998; Vrielynck and Bouysse, 2001), or to a change from a transtensional to a distensional regime in the Neotethys accretion system (Ricou, 1994). Both processes might lead to a reactivation of the extensional tectonic structures inherited from the Permian breakup. The resulting extension might have caused convective thinning of the subcontinental lithosphere similarly to that in the Basin and Range province (Fitton et al., 1991; DePaolo and Daley, 2000). We suggest that this thinning led to the decompression-triggered partial melting of the Arabian uprising mantle, and to the emplacement of the Triassic Hawasina basalts.

6. Conclusions

1. Middle to Late Triassic volcanic rocks from the Hawasina Nappes are predominantly alkali basalts, with minor associated sub-alkaline basalts, trachyandesites, trachytes and rhyolites. Most of them are geochemically very similar to the more abundant Permian plume-related high-Ti basalts, which also occur in the Hawasina Nappes.

2. The Triassic basalts derive from low-degree melting of an enriched OIB-type mantle source, characterized by $0.3 < \varepsilon Nd_i < 5.3$ and $^{206}Pb/^{204}Pb_i$ =16.96-19.31. With time, the degree of partial melting increased and the corresponding depths decreased from the garnet + spinel to the spinel lherzolite facies. Some of the oldest and deepest melts (UmV_1 unit of Umar Group) are distinguished from the others by their unradiogenic Nd and Pb signature, with -

$4.5 < \varepsilon Nd_i < -1.2$ and $^{206}Pb/^{204}Pb_i$ =16.35-17.08. We attribute these features to contamination by the lower continental crust of the Oman margin.

3. The Triassic Hawasina lavas show no evidence for a depleted mantle source, such as those documented for the Permian tholeiitic low-Ti basalts of Oman and the Triassic oceanic island-type tholeiites of Cyprus. The ca. 35 My time span between their emplacement and that of their Permian equivalents suggests that they were not related to prolonged activity of the Tethyan plume. We propose instead that they originated from the partial melting of the Oman lithospheric mantle, the original DM-HIMU signature of which was overprinted during its pervasive metasomatism by Permian plume-related melts.

4. The origin of the Hawasina Triassic volcanism is tentatively attributed to a post-breakup decompression-triggered melting event linked to an extensional remobilization of the earlier tectonic structures of the Oman margin. This remobilization was possibly a consequence of the global kinematic reorganization of the Tethyan realm during the Middle Triassic.

Acknowledgements

This study was initiated by the late Professor Jean Marcoux, Université de Paris 7, who communicated to us his enthusiasm for the study of the Tethyan margin in Oman. It was funded by the Institut National des Sciences de la Terre, programme “Intérieur de la Terre”, the Groupement de Recherche “Marges”, CNRS UMR 5025 (Université Joseph Fourier, Grenoble) and UMR 6538 (Université de Bretagne Occidentale, Brest), and the BRGM Research Division. Critical comments by Drs. Sobhi Nasir, Michel Grégoire and an anonymous reviewer, together with editorial comments by Dr. Andrew Kerr, led to considerable shortening and improvement of the initial manuscript. We also thank Nick Arndt for checking the revised version. We acknowledge the authority of Oman and especially thank Dr. Hilal Mohammed Sultan Al Azry, Director of the Geological Survey, Omani Ministry of Commerce and Industry, for his welcome and support in Oman. Dr. François Béchennec is thanked for his contribution to field studies, stimulating discussions and useful comments on the manuscript.

References

Ahmad, T., Islam R., Khanna, P.P., Thakur, V.C., 1996. Geochemistry, petrogenesis and tectonic significance of the basic volcanic units of the Zildat ophiolitic mélange, Indus suture zone, eastern Ladakh (India). Geodinamica Acta 9, 222-233.

Al Riyami, K., Robertson, A.H.F., 2002. Mesozoic sedimentary and magmatic evolution of the Arabian continental margin, northern Syria: evidence from the Baer-Bassit Melange. Geological Magazine 139, 395-420.

Altherr, R., Henjes-Kunst, F., Baumann, A., 1990. Asthenosphere versus lithosphere as possible sources for basaltic magmas erupted during formation of the Red Sea: constraints from Sr, Pb and Nd isotopes. Earth and Planetary Science Letters 96, 269-286.

Andersson, U.B., Ghebreab, W., Teklay, M., 2006. Crustal evolution and metamorphism in east-Eritrea south-east Arabian-Nubian Shield. Journal of African Earth Sciences 44, 45-65.

Baker, J. A., Menzies, M.A., Thirlwall, M.F., Macpherson, C.G., 1997. Petrogenesis of Quaternary intraplate volcanism, Sana'a, Yemen: implications for plume lithosphere interaction and polybaric melt hybridization. Journal of Petrology 38, 1359-1390.

Baker, J.A., Macpherson, C.G., Menzies, M.A., Thirlwall, M.F., Al-Kadasi, M., Mattey, D.P., 2000. Resolving crustal and mantle contributions to continental flood volcanism, Yemen: Constraints from mineral oxygen isotope data. Journal of Petrology 41, 1805-1820.

Baker, J.A., Chazot, G., Menzies, M A., Thirlwall, M., 2002. Lithospheric mantle beneath Arabia: A Pan-African protolith modified by the Afar and older plumes, rather than a source for continental volcanism? In: Menzies, M.A., Klemperer, S.L., Ebinger, C.J., Baker, J. (Eds.), Volcanic Rifted Margins. Geological Society of America Special Paper, vol. 362, pp. 65-80.

Barrat, J.A., Keller. F., Amossé, J., 1996. Determination of rare earth elements in sixteen silicate reference samples by ICP-MS after Tm addition and ion exchange separation. Geostandard Newsletter 20, 133-139.

Basile, C., Chauvet, F., 2009. Hydromagmatic eruption during the buildup of a Triassic carbonate platform (Oman Exotics): eruptive style and associated deformations. Journal of Volcanology and Geothermal Research 183, 84-96.

Baud, A., Béchennec, F., Cordey, F., Krystyn, L., Le Métour, J., Marcoux, J., Maury, R., Richoz, S., 2001. Permo-Triassic deposits: from the platform to the basin and seamounts. International Conference on the Geology of Oman, Excursion, n°A01, 56 p.

Béchennec, F., 1987. Géologie des Nappes Hawasina dans les parties orientale et centrale des Montagnes d'Oman. Thèse Doctorat d'Etat, Université Pierre et Marie Curie, Paris VI, Document du BRGM 127, 474 p.

Béchennec, F., Le Métour, J., Platel, J.P., Roger, J., 1993. Geological map of the Sultanate of Oman, scale 1/1000000, Explanatory notes; Sultanat of Oman. Ministry of Petroleum and Minerals, Directorate General of Minerals (Ed.).

Béchennec, F., Le Métour, J., Rabu, D., Villet, M., Beurrier, M., 1988. The Hawasina Basin: a fragment of a starved passive continental margin, thrust over the Arabian Platform during obduction of the Sumail Nappe. Tectonophysics 151, 323-343.

Béchennec, F., Le Métour, J., Rabu, D., Bourdillon-Jeudy de Grissac, C., De Wever, P., Beurrier, M., Villet, M., 1990. The Hawasina Nappes: stratigraphy, paleogeography and structural evolution of a fragment of the south-Tethyan passive continental margin. In: Robertson, A.H.F., Searle, M.P., Ries, A.C. (Eds.), The Geology and Tectonics of the Oman Region. Geological Society Special Publication 49, pp. 213-223.

Béchennec, F., Tegyey, M., Le Métour, J., Lemière, B., Lescuyer, J.L., Rabu, D., Milési, J.P., 1991. Igneous rocks in the Hawasina nappes and the Al-Hajar supergroup, Oman mountains: their significance in the birth and evolution of the composite extensional margin of eastern Tethys. In: Peters, T., Nicolas, A., Coleman, R.G. (Eds.), Ophiolite genesis and evolution of the oceanic lithosphere. Ministry of Petroleum and Minerals, Directorate General of Minerals of Oman, Kluwer, pp. 569-611.

Bertrand, H., Chazot, G., Blichert-Toft, J., Thoral, S., 2003. Implications of widespread high-μ volcanism on the Arabian Plate for Afar mantle plume and lithosphere composition. Chemical Geology 198, 47-61.

Bernouilli, D., Weissert, H., 1987. The upper Hawasina nappes in the central Oman mountains: stratigraphy, palinspatics and sequence of nappes emplacement. Geodinamica Acta 1, 47-58.

Besse, J., Torcq, F., Gallet, Y., Ricou, L.E., Krystyn, L., Saidi, A., 1998. Late Permian to Late Triassic paleomagnetic data from Iran: constraints on the migration of the Iranian block through the Tethyan Ocean and initial destruction of Pangaea. Geophysical Journal International 135, 77-92.

Beurrier, M., Béchennec, F., Rabu, D., Hutin, G., 1986. Geological map of Rustaq: Sheet NF40-3A, Scale 1/100 000, Sultanate of Oman. Ministry of Petroleum and Minerals, Directorate General of Minerals (Ed.).

Blusztajn, J., Hart, S.R., Shimizu, N., McGuire, A.V., 1995. Trace element and isotopic characteristics of spinel peridotite xenoliths from Saudi Arabia. Chemical Geology 123, 53-65.

Bosch, D., Blichert-Toft J., Moynier, F., Nelson, B.K., Telouk, P., Gillot, P.Y., Albarède, F., 2008. Pb, Hf and Nd isotope compositions of the two Réunion volcanoes, Indian Ocean: a tale of two small-scale mantle "blobs". Earth and Planetary Science Letters 265, 748-768.

Caroff, M., Maury, R.C., Guille, G., Cotten, J., 1997. Partial melting below Tubuai (Austral Islands, French Polynesia). Contributions to Mineralogy and Petrology 127, 369–382.

Chan, G.H.-N., Malpas, J., Xenophontos, C., Lo, C.-H., 2008. Magmatism associated with Gondwanaland rifting and Neo-Tethyan oceanic basin development: evidence from the Mamonia Complex, SW Cyprus. Journal of the Geological Society London 165, 699-709.

Chauvel, C., McDonough, W., Guille, G., Maury, R.C., Duncan, R., 1997. Contrasting old and young volcanism in Rurutu Island, Austral chain. Chemical Geology 139, 125-143.

Chauvel, C., Blichert-Toft, J., 2001. A hafnium isotope and trace element perspective on melting of the depleted mantle. Earth and Planetary Science Letters 190, 137-151.

Chauvet, F., Lapierre, H., Bosch, D., Guillot, S., Mascle, G., Vannay, J.-C., Cotten, J., Brunet, P., Keller, F., 2008. Geochemistry of the Panjal Traps basalts (NW Himalaya): records of the Pangea Permian break-up. Bulletin de la Société Géologique de France 179, 383 - 395.

Cohen, R.S., O'Nions, R.K., Dawson, J.B., 1984. Isotope geochemistry of xenoliths from East Africa: implications for development of mantle reservoirs and their interaction. Earth Planetary Science Letters 68, 209-220.

Coleman, R.G., 1981. Tectonic setting for ophiolite obduction in Oman. Journal of Geophysical Research 86, 2497-2508.

Corfield, R.I., Searle, M.P., Green, O.R., 1999. Photang thrust sheet: an accretionary complex structurally below the Spongtang ophiolite constraining timing and tectonic environment of ophiolite obduction, Ladakh Himalaya, NW India. Journal of the Geological Society London 156, 1031-1044.

Cotten, J., Le Dez, A., Bau, M., Caroff, M., Maury, R.C., Dulski, P., Fourcade, S., Bohn, M., Brousse, R., 1995. Origin of anomalous rare-earth element and yttrium enrichments in subaerially exposed basalts: evidence from French Polynesia. Chemical Geology 119, 115-138.

Davidson, J. P., Wilson, I. R., 1989. Evolution of an alkali basalt-trachyte suite from Jebel Marra volcano, Sudan, through assimilation and fractional crystallization. Earth and Planetary Science Letters 95, 141-160.

DePaolo, D.J., 1980. Trace element and isotopic effects of combined wallrock assimilation and fractional crystallization, Earth and Planetary Science Letters 53, 189-202.

DePaolo, D.J., Daley, E.E., 2000. Neodymium isotopes in basalts of the southwest basin and range and lithospheric thinning during continental extension. Chemical Geology 169, 157-185.

Dercourt, J., Ricou, L.E., Vrielynk, B. (Eds.), 1993. Atlas Tethys Palaeoenvironmental Maps. Gauthier-Villars, Paris, 14 maps.

De Wever, P., Bourdillon de Grissac, C., Bechennec F., 1990. Permian to Cretaceous radiolarian biostratigraphic data from the Hawasina Complex, Oman Mountains. In: Robertson, A.H.F., Searle, M.P., Ries, A.C. (Eds.), The Geology and Tectonics of the Oman Region. Geological Society Special Publication 49, pp. 225-238.

Downes, H., 2001. Formation and modification of the shallow sub-continental lithospheric mantle: a review of geochemical evidence from ultramafic xenolith suites and tectonically emplaced ultramafic massifs of western and central Europe. Journal of Petrology 42, 233-250.

Dupuy, C., Vidal, P., Maury, R.C., Guille, G., 1993. Basalts from Mururoa, Fangataufa and Gambier islands (French Polynesia): geochemical dependance on the age of the lithosphere. Earth Planetary Science Letters 117, 89-100.

Fitton, J.G., James, D., Leeman, W.P., 1991. Basic magmatism associated with Late Cenozoic extension in the western United States: compositional variations in space and time. Journal of Geophysical Research 96 (B8), 13,693-13,711.

Fitton, J.G., Saunders, A.D., Norry, M.J., Hardarson, B.S., Taylor, R.N., 1997. Thermal and chemical structure of the Iceland plume. Earth and Planetary Science Letters 153, 197-208.

Garzanti, E., Le Fort, P., Sciunnach, D., 1999. First report of Lower Permian basalts in South Tibet: tholeiitic magmatism during break-up and incipient opening of Neotethys. Journal of Asian Earth Sciences 17, 533-546.

Gibson, S.A., Thompson, R.N., Dickin, A.P., Leonardos, O.H., 1995. High-Ti and low-Ti mafic potassic magmas: Key to plume-lithosphere interactions and continental flood-basalt genesis. Earth and Planetary Science Letters 136, 149-165.

Glennie, K.W., Bœuf, M.G.A., Hughes Clarke, M.W., Moody-Stuart, M., Pilaart, W.F.H., Reinhardt, B.M., 1974. Geology of the Oman moutains. Geologie en Mijnbouw, 1,423 p.

Hamelin, B., Allègre, C. J., 1988. Lead isotope study of orogenic lherzolite massifs. Earth and Planetary Science Letters 91, 117-131.

Harry, D.L., Leeman, W.P., 1995. Partial melting of melt metasomatized subcontinental mantle and the magma source potential of the lower lithosphere. Journal of Geophysical Research 100 (B7), 10,255-10,269.

Hart, S. R., 1984. A large isotope anomaly in the Southern Hemisphere mantle. Nature 309, 753-757.

Hawkesworth, C. J., Kempton, P. D., Rogers, N. W., Ellam, R. M., van Calsteren, P. W., 1990. Continental mantle lithosphere, and shallow level enrichment processes in the Earth's mantle. Earth and Planetary Science Letters 96, 256-268.

Hawkesworth, C.J., Gallagher, K., Kelley, S., Mantovani, M., Peate, D.W., Regelous, M, Rogers, N.W., 1992. Paraná magmatism and opening of the South Atlantic. In: Storey, B.C. Alabaster, T., Pankhurst, R.J. (Eds.), Magmatism and the causes of continental break up. Geological Society Special Publication 68, pp. 221-240.

Hegner, E., Pallister, J.S., 1989. Pb, Sr, and Nd isotopic characteristics of Tertiary Red Sea rift volcanics form the central Saudi Arabian coastal plain. Journal of Geophysical Research, 94, 7749-7755.

Hoernle, K., Zhang, Y.S., Graham, D., 1995. Seismic and geochemical evidence for large-scale mantle upwelling beneath the eastern Atlantic and western and central Europe. Nature 374, 34-39.

Kokfelt, T.F., Hoernle, K., Hauff, F., Fiebig, J., Werner, R., Garbe-Schönberg, D., 2006. Combined trace element and Pb-Nd-Sr-O isotope evidence for recycled oceanic crust (upper and lower) in the Iceland mantle plume. Journal of Petrology 47, 1705-1749.

Lancelot, J.R., Bosch, D., 1991. A Pan-African age for the HP-HT granulite gneisses of Zabargad island: implications for the early stages of the Red Sea rifting. Earth and Planetary Science Letters 107, 539-549.

Lapierre, H., Bosch, D., Narros, A., Mascle, G. H., Tardy, M., Demant A., 2007. The Mamonia Complex (SW Cyprus) revisited: remnant of Late Triassic intra-oceanic volcanism along the Tethyan southwestern passive margin. Geological Magazine 144, 1-19.

Lapierre, H., Dupuis, V., Mercier De Lepinay, B., Tardy, M., Ruiz, J., Maury, R.C., Hernandez, J., Loubet, M., 1997. Is the lower Duarte igneous complex (Hispaniola) a remnant of the Caribbean plume-generated oceanic plateau ? Journal of Geology 105(1), 111-120.

Lapierre, H., Samper, A., Bosch, D., Maury, R.C., Bechennec, F., Cotten, J., Demant, A., Brunet, P., Keller, F., Marcoux, J., 2004. The Tethyan plume: geochemical diversity of Middle Permian basalts from the Oman rifted margin. Lithos 74, 167-198.

Le Bas, M.J., Le Maitre, R.W., Streickheisen, A., Zanettin, B., 1986. A chemical classification of igneous rocks based on the total-alkali-silica diagram. Journal of Petrology 27, 745-750.

Lightfoot, P.C., Hawkesworth, C.J., Hergt, J., Naldrett, A.J., Gorbatchev, N.S., Fedorenko, V.A., Doherty, W. 1993. Remobilisation of the continental lithosphere by a mantle plume: major- trace- element, and Sr- Nd- and Pb-isotope evidence from picritic and tholeiitic lavas of the Noril'sk District, Siberian Traps, Russia. Contributions to Mineralogy and Petrology 114, 171-188.

Lippard, S.J., Shelton, A.W., Gass, I.G., 1986. The Ophiolite of northern Oman. Geological Society of London, Memoir 11, 178 pp.

Luhr, J.F., Aranda-Gómez, J.J., Housh, T.B., 1995. San Quintín Volcanic Field, Baja California Norte, México. Geology, petrology and geochemistry. Journal of Geophysical Research 100 (B7), 10353–10380.

MacDonald, G. A., Katsura, T., 1964. Chemical composition of Hawaiian lavas. Journal of Petrology 5, 82-133.

Maury, R.C., Béchennec, F., Cotten, J., Caroff, M., Cordey, F., Marcoux, J., 2003. Middle Permian plume-related magmatism of the Hawasina Nappes and the Arabian Platform: implications on the evolution of the Neotethyan margin in Oman. Tectonics 22 (6), 1073, doi:10.129/2002TC001483.

Maury, R.C., Lapierre, H., Bosch, D., Marcoux, J., Krystyn, L., Cotten, J., Bussy, F., Brunet, P., Sénebier, F., 2008. The alkaline intraplate volcanism of the Antalya Nappes (Turkey): a Late Triassic remnant of the Neotethys. Bulletin de la Société géologique de France 179, 397-410.

McDonough, W.F., 1990. Constraints on the composition of the continental lithospheric mantle. Earth and Planetary Science Letters 101, 1-18.

McLennan, S., 2001. Relationships between the trace element composition of sedimentary rocks and upper continental crust. Geochemistry Geophysics Geosystems 2, paper number 2000GC000109.

Monjoie, P., Lapierre, H., Tashko, A., Mascle, G.H., Dechamp, A., Muceku, B., Brunet, P., 2008. Nature and origin of the Triassic volcanism in Albania and Othrys: a key to understanding the NeoTethys opening? Bulletin de la Société géologique de France 179, 411-425.

Peate, D.W., Hawkesworth, C.J., 1996. Lithospheric to Asthenospheric transition in Low-Ti flood basalts from southern Parana, Brazil, Chemical Geology 127, 1-24.

Perez, C., 2006. Le magmatisme de la marge arabique au Trias et Jurassique: analyses pétrogéochimiques dans la région du Baër-Bassit (Syrie) et implications géodynamiques. Mem. M2R, Univ. J. Fourrier, Grenoble, 46 p.

Phipps Morgan, J., Morgan, W.J., 1999. Two-stage melting and the geochemical evolution of the mantle: a recipe for mantle plum-pudding. Earth and Planetary Science Letters 170, 215-239.

Pik, R., Deniel, C., Coulon, C., Yirgu, G., Hofmann, C., Ayalew, D., 1998. The Northwestern Ethiopian plateau flood basalts: Classification and spatial distribution of magma types. Journal of Volcanology Geothermal Research 81, 91–111.

Pik, R., Deniel, C., Coulon, C., Yirgu, G., Marty, B., 1999. Isotopic and trace element signatures of Ethiopian flood basalts: Evidence for plume–lithosphere interactions. Geochimica Cosmochimica Acta 63(15), 2263–2279.

Pillevuit, A., 1993. Les Blocs Exotiques du Sultanat d'Oman, Mémoires de Géologie, Lausanne vol. 17, 249 p.

Pillevuit, A., Marcoux, J., Stampfli, G., Baud, A., 1997. The Oman Exotics: a key for the understanding of the Neotethyan geodynamic evolution. Geodinamica Acta 10 (5), 209-238.

Raffone, N., Chazot, G., Pin, C., Vanucci, R., Zanetti, A., 2009. Metasomatism in the lithospheric mantle beneath Middle Atlas (Morocco) and the origin of Fe- and Mg-rich wehrlites. Journal of Petrology 50, 197-249.

Ricou, L.E., 1994. Tethys reconstructed: plates, continental fragments and their boundaries since 260 My from Central America to South-Eastern Asia. Geodinamica Acta 7, 169-218.

Robertson, A.H.F., Searle, M.P., 1990. The northern Oman Tethyan continental margin: stratigraphy, structure, concepts and controversies. In: Robertson, A.H.F., Searle, M.P., Ries, A.C., (Eds.), The Geology and Tectonics of the Oman Region. Geological Society Special Publication No. 49, pp. 3-25.

Robertson, A.H.F., 1998. Rift-related sedimentation and volcanism of the north-Indian margin inferred from a Permian-Triassic exotic block at Lamayuru, Indus suture zone (Ladakh Himalaya) and regional comparisons. Journal of Asian Earth Sciences 16, 159-172.

Saidi, A., Brunet, M.F., Ricou, L.E., 1997. Continental accretion of the Iran Block to Eurasia as seen from the Late Paleozoic to Early Cretaceous subsidence curves. Geodinamica Acta 10, 189-208.

Saunders, A.D., Storey, M., Kent, R.W., Norry, M.J., 1992. Consequences of plume-lithosphere interactions. In: Storey, B.C., Alabaster, T., Pankhurst, R.J. (Eds.), Magmatism and the causes of continental break up. Geological Society Special Publication No. 68, pp. 41-60.

Searle, M.P. Lippard, S.J., Smewing, D.J., Rex, D.C. 1980. Volcanic rocks beneath the Semail ophiolite nappe. Geological Society London, 137,589-604

Searle, M.P., Graham, G.M., 1982. "Oman exotics" - Oceanic carbonate build-ups associated with the early stages of continental rifting. Geology 10, 43-49.

Sharma, M., 1997. Siberian Traps. In Mahoney J., Coffin M.F. (eds), Large igneous provinces: Continental oceanic and planetary flood volcanism. American Geophysical Union Geophysical Monograph 100, 273-295.

Shaw, J.E., Baker, J.A., Kent, A.J.R., Ibrahim, K.M., Menzies, M.A., 2007. The Geochemistry of the Arabian Lithospheric Mantle: a Source for Intraplate Volcanism? Journal of Petrology 48, 1495-1512.

Stampfli, G.M., Marcoux, J., Baud, A., 1991. Tethyan margins in space and time. Paleogeography Paleoclimatology Paleoecology 87, 373-409.

Stampfli, G.M., Borel, G.D., 2002. A plate tectonic model for the Paleozoic and Mesozoic constrained by dynamic plate boundaries and restored synthetic oceanic isochrons. Earth Planetary Science Letters 196, 17-33.

Stein, M., Goldstein, S. L., 1996. From plume head to continental lithosphere in the Arabian-Nubian shield. Nature 382, 773-778.

Stern, R.J., 1994. Arc assembly and continental collision in the Neoproterozoic east african orogen: implications for the consolidation of Gondwanaland. Annual Revue of Earth Planetary Science Letters 22, 319-351.

Stoeser, D.B., Frost, C.D., 2006. Nd, Pb, Sr, and O isotopic characterization of Saudi Arabian Shield terranes. Chemical Geology 226, 163-188.

Sun, S.S., McDonough, W.F., 1989. Chemical and isotopic systematics of oceanic basalts: implication for mantle composition and processes. In: Saunders, A.D., Norry, M.J. (Eds.), Magmatism in the Ocean Basins. Geological Society Special Publication 42, pp. 313-345.

Vrielynck, B., Bouysse, P., 2001. Le visage changeant de la Terre. L'éclatement de la Pangée et la mobilité des continents au cours des derniers 250 millions d'années. Publication de la Commission de la Carte Géologique du Monde, Paris, 32 p.

Watts, K.F., 1990. Mesozoic carbonate slope facies marking the Arabian platforme margin in Oman: depositional history, morphology and palaeogeography. In: Robertson, A.H.F., Searle, M.P., Ries, A.C. (Eds.), The Geology and Tectonics of the Oman Region. Geological Society Special Publication 49, pp. 127-138.

Whitehouse, M.J., Windley, B.F., Stoeser, D.B., Al-Khirbash, S., Mahfood, A.O., Ba-Bttat, Haider, A., 2001. Precambrian basement character of Yemen and correlations with Saudi Arabia and Somalia. Precambrian Research 105, 357–369.

Willbold, M., Stracke, A., 2006. Trace element composition of mantle end-members: implications for recycling of oceanic and upper and lower continental crust. Geochemistry Geophysics Geosystems 7, Q04004, doi:10.1029/2005GC001005.

Wilson M., 1989. Igneous petrogenesis, a global tectonic approach. Chapman and Hall publishers, London.

Winchester, J.A., Floyd, P.A., 1977. Geochemical discrimination of different magma series and their different products using immobile elements. Chemical Geology 20, 325-343.

Zindler, A., Hart, S.R., 1986. Chemical systematics. Annual Review of the Earth and Planetary Sciences 14, 493-571.

Figure captions

Fig. 1. Geological setting. a) The Tethyan Suture (ophiolites and associated mélanges) after Coleman (1981), with locations of the main late Carboniferous, Permian and Triassic volcanic sequences associated to the Neotethyan margins inverted segments (mainly from Garzanti et al., 1999). b) Simplified geological map of the Oman Mountains and associated main structural units (after Glennie et al., 1974). c) Sampling locations on the geological map of the Hawasina nappes (after Béchennec, 1987 modified by de Wever et al., 1990). Sampling sites coordinates of Sinni: 23°25’4’’N - 57°09’2’’E; Sayjah: 23°11’23’’N - 57°51’58’’E; Aqil: 22°47’8’’N - 57°48’4’’E (Om-45); 22°47’2’’N - 57°51’3’’E (Om-52); 22°47’5’’N - 57°48’2’’E (Om-42); 22°47’9’’N - 57°48’4’’E (Om-48 and -49); Jabal Buwaydah 1: 22°53’6’’N - 57°05’7’’E; Jabal Buwaydah 2: 23°00’8N - 57°00’E. d) Regional cross section according to Béchennec (1987).

Fig. 2. Selected major element plots for the Triassic Hawasina basin lavas. a) MgO (wt.%), b) TiO_2 (wt.%) and c) Na_2O+K_2O (wt.%) *versus* SiO_2 (wt.%) plots. The trend separating alkaline and tholeiitic fields in c) is from MacDonald and Katsura (1964) and the lava nomenclature from Le Bas et al. (1986).

Fig. 3. Chondrite and primitive mantle-normalized trace elements patterns of (a) Umar Group samples. b) Comparison between multielement patterns of selected Kawr and Alridh Groups basalts and trachybasalts with OIB patterns and the compositional field of the alkaline Umar Group samples from the Al Qurti UmV_1 unit and the Sinni village (grey array). Chondrite, primitive mantle and OIB compositions are from Sun and McDonough (1989).

Fig. 4. a) Zr/Ti *versus* Nb/Y discriminating diagram of Winchester and Floyd (1977). b) Plot of Triassic Hawasina basalts and trachybasalts in the Nb/Y *versus* Zr/Y diagram of Fitton et al. (1997) together with Iceland plume-related picritic, tholeiitic and alkaline primary basalts (MgO > 8 wt.%) of the Neo-Volcanic Zone, and the Kolbeinsey and Reykjanes ridge basalts (Kokfelt et al., 2006). Note the deviation towards low Nb/Y values for samples with La/Nb < 1.

Fig. 5. Initial Pb and Nd isotopic compositions of Triassic Hawasina lavas. Plots of a) $(^{207}Pb/^{204}Pb)_i$, b) $(^{208}Pb/^{204}Pb)_i$ and c) εNdi against $(^{206}Pb/^{204}Pb)_i$. The compositional fields of Indian and Atlantic MORB are compiled from the Petrological Database of the Ocean Floor (PETDB). Compositional fields of OIB, mantle isotopic components HIMU (for High-μ), EM 1 and EM 2 (for Enriched Mantle 1 and 2) and the NHRL (Northern Hemisphere Reference Line) are from Zindler and Hart (1986).

Fig. 6. a) and b) Al_2O_3 (wt.%) and Eu/Eu* *versus* SiO_2 (wt.%) diagrams for Al Qurti samples of the Umar Group c) $(La/Yb)_N$ ratios of Al Qurti samples plotted against their stratigraphic position. d) and e) $(La/Yb)_N$ *versus* La(ppm) and εNd_i *versus* SiO_2 (wt.%) diagrams for all Triassic Hawasina samples.

Fig. 7. Selected REE plots. a) and b) $(La/Yb)_N$ and La *versus* $(Sm/Yb)_N$ plots for Hawasina Triassic basalts and trachybasalts. The meaning of arrows (1) and (2) is explained in the text. c) La/Yb and Yb (ppm) variations during non-modal partial melting (F values: partial melting degrees) of garnet and spinel lherzolite sources "s" containing different proportions of these minerals (100% Gt – 0% Sp, 50 % - 50 %, 30% - 70%, 0% Gt – 100% Sp). In this model developed by Luhr et al. (1995), source "s" is assumed to be enriched relative to chondrite, with La = 6 * Ch (1.79 ppm) and Yb = 1.5 * Ch (0.31 ppm). This model was used by Luhr et al. (1995) for primitive basalts with Mg# > 68 to limit the fractionation effects related to magmatic differentiation. As the iron contents of the studied basalts may have been modified by post-magmatic processes, their MgO contents are used to check the

primitive character Hawasina Triassic basalts. Samples with MgO > 7 wt.% are identified by thick and doubled symbols.

Fig. 8. Plots of the εNd_i of Triassic Hawasina basalts and trachybasalts against: a) La/Nb; b) Th/Nb; c) $(La/Sm)_N$ and d) Ti/Y. MORB and OIB compositions are from Sun and McDonough (1989). SCLM (Sub-Continental Lithospheric Mantle) composition is from McDonough (1990) and the compositions of LC and UC (Lower and Upper continental Crust) from McLennan (2001).

Fig. 9. Nd and Pb isotopic compositions of Triassic Hawasina volcanics recalculated at t = 230 My, compared to the published fields of the Arabian sub-continental lithospheric mantle and the regional upper and lower crusts. E. Pr.: Early Proterozoic, Ar: Archean, L. Ar.: Late Archean. MORB, OIB, EM 1 and EM 2 are from Zindler and Hart (1986); NHRL is from Hart (1984); Arabian lithospheric mantle is from Shaw et al. (2007 - Jordan), Baker et al. (2002, 1997 – Yemen and Southern Red Sea), Hamelin and Allègre (1988 – Zabargad Island), Blusztajn et al. (1995 – Saudi Arabia). Sudanese crust is from Davidson and Wilson (1989); Yemen and Saudi Arabia upper crust is from Whitehouse et al. (2001); Baker et al. (2000); Hegner and Pallister (1989); the lower mafic crust is from Cohen et al. (1984 - Tanzania), Altherr et al. (1990) and G. Chazot and J. A. Baker (unpublished data presented as a composition field in Baker et al., 1997 – Arabia and Yemen); the gneissic lower crust is from Lancelot and Bosch (1991 – Zabargad Island).

Fig. 10. Nd and Pb isotopic compositions (at t = 230 My) of Triassic intraplate volcanic sequences from Oman and the Eastern Mediterranean occurrences. Data are from this work (Oman); Lapierre et al., 2007 (Cyprus); Maury et al., 2008 (Turkey); Perez, 2006 (Syria); Monjoie et al., 2008 (Greece).

Fig. 11. Geochemical comparison between the Permian and Triassic lavas from the Oman margin. All Permian data are from Lapierre et al. (2004) and Maury et al. (2003). a) and b) plots of TiO_2 (wt.%) and $(La/Sm)_N$ *versus* Th (ppm) for basalts from the two magmatic events. c) Primitive mantle-normalized multielement patterns of the Permian Groups 1, 2 and 3 and of the Triassic basalts and trachybasalts.

Fig. 12. a) and b) Plots of $\varepsilon(Nd)_i$ values *versus* $(La/Sm)_N$ and La/Nd ratios for the Permian Groups 1, 2 and 3 (Lapierre et al., 2004) and the Triassic basalts and trachybasalts. c) $\varepsilon(Nd)_i$ *versus* $(^{206}Pb/^{204}Pb)_i$ diagrams. All isotopic data are recalculated at t = 230 My. The meaning

of A, B, C and D in diagrams a) and b) is explained in the text. MORB, OIB and primitive mantle reference values are from Sun and McDonough (1989).

Table captions

Table 1. Major element (wt.%) and trace element (ppm) compositions of representative Triassic lavas (whole set shown in Appendix A). Trace element compositions measured by ICP-AES are shown in italics and those obtained by ICP-MS in normal numbers. B: basalts (SiO_2 < 53 wt.% and MgO > 6 wt.%); TB: trachybasalts (SiO_2 < 53 wt.% and MgO = 3 to 6 wt.%); DB: basaltic dolerite; TA: trachyandesite; T: trachyte; R: Rhyolite. Analytical methods explained in the text.

Table 2. Nd and Pb actual and initial ("i" for t = 230 My) isotopic compositions with their incertitudes (± 2 σ) for Triassic volcanics from the Hawasina nappes. Analytical methods explained in the text.

Appendix

Appendix A. Selected sampling sites. a) Cross section and sample locations in the Al Qurti site of the Umar Group (Fig. 1c). b) Stratigraphic column of the basal 300 m of the Kawr Group at Jabal Misfah (Fig. 1c) and location of samples.

Appendix B. Major element and trace element compositions of Triassic lavas from the Hawasina Nappes. Trace element compositions measured by ICP-AES are shown in italics and those obtained by ICP-MS in normal numbers. B: basalts (SiO_2 < 53 wt.% and MgO > 6 wt.%); TB: trachybasalts (SiO_2 < 53 wt.% and MgO > 3 wt.%); DB: basaltic dolerite; TA: trachyandesite; T: trachyte; R: Rhyolite. Analytical methods explained in the text.

Appendix C. Chondrite and primitive mantle-normalized trace elements patterns of Middle to Late Triassic lavas from the Hawasina Nappes. Chondrite and primitive-mantle compositions are from Sun and McDonough (1989).

Appendix D. Plots of La, Nd, Sm, U and Pb against Th (ppm) for Triassic Hawasina samples. The linear trends reported on some diagrams correspond to the average Th/U and Th/Pb ratios of OIB (Sun and McDonough, 1989).

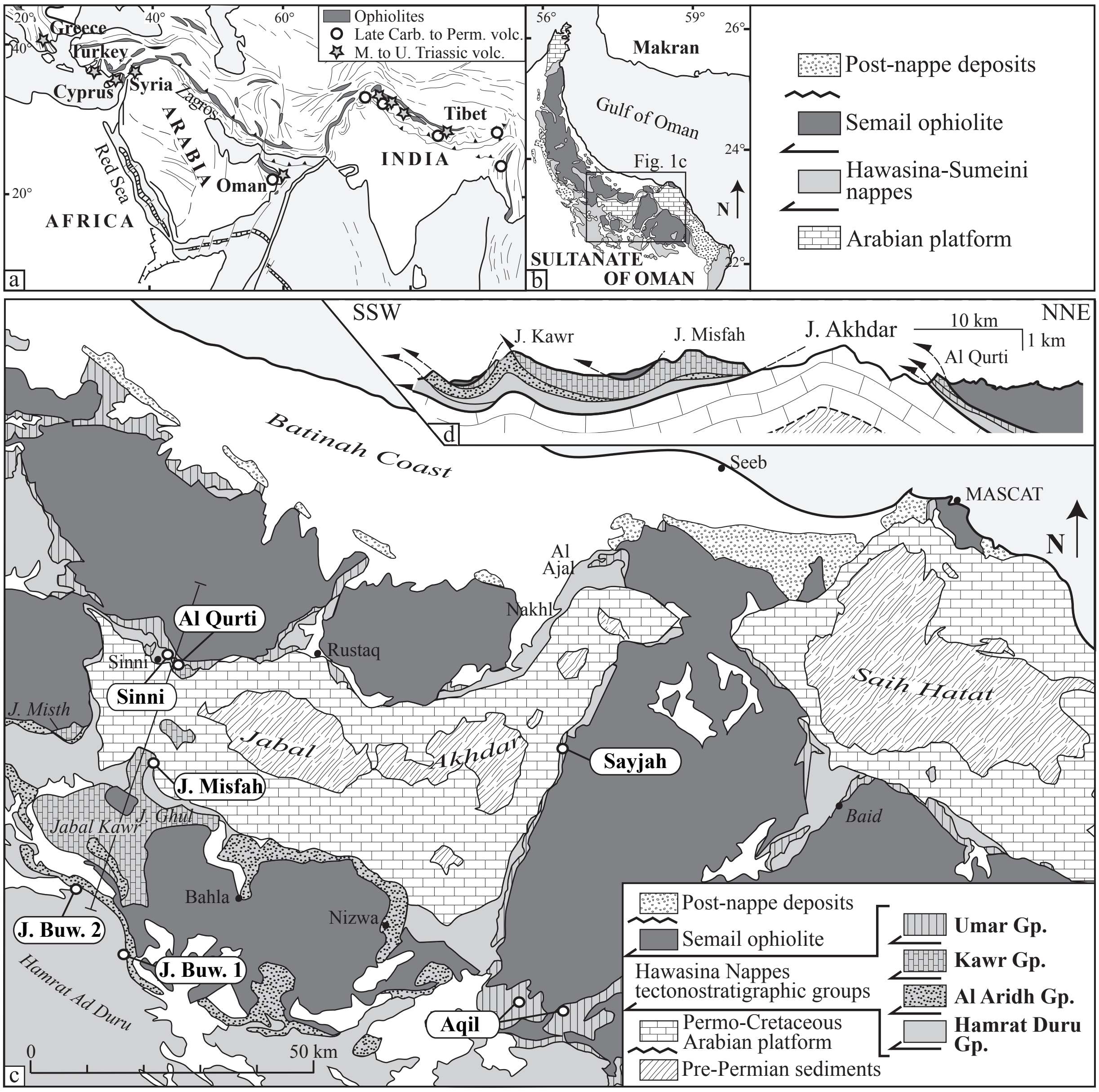

Ophiolites
Late Carb. to Perm. volc.
M. to U. Triassic volc.
Greece
Turkey
Cyprus
Syria
Zagros
ARABIA
Red Sea
AFRICA
Oman
INDIA
Tibet
20°
40°
60°
a
56°
59°
26°
24°
22°
Makran
Gulf of Oman
Fig. 1c
N
SULTANATE OF OMAN
b
Post-nappe deposits
Semail ophiolite
Hawasina-Sumeini nappes
Arabian platform
SSW
NNE
J. Kawr
J. Misfah
J. Akhdar
10 km
1 km
Al Qurti
d
Batinah Coast
Seeb
MASCAT
N
Al Ajal
Nakhl
Al Qurti
Sinni
Rustaq
J. Misth
Jabal
Akhdar
Saih Hatat
Sayjah
J. Misfah
Jabal Kawr
J. Ghul
Baid
Bahla
Nizwa
J. Buw. 2
J. Buw. 1
Hamrat Ad Duru
Aqil
0
50 km
c
Post-nappe deposits
Semail ophiolite
Hawasina Nappes tectonostratigraphic groups
Permo-Cretaceous Arabian platform
Pre-Permian sediments
Umar Gp.
Kawr Gp.
Al Aridh Gp.
Hamrat Duru Gp.

Fig. 1

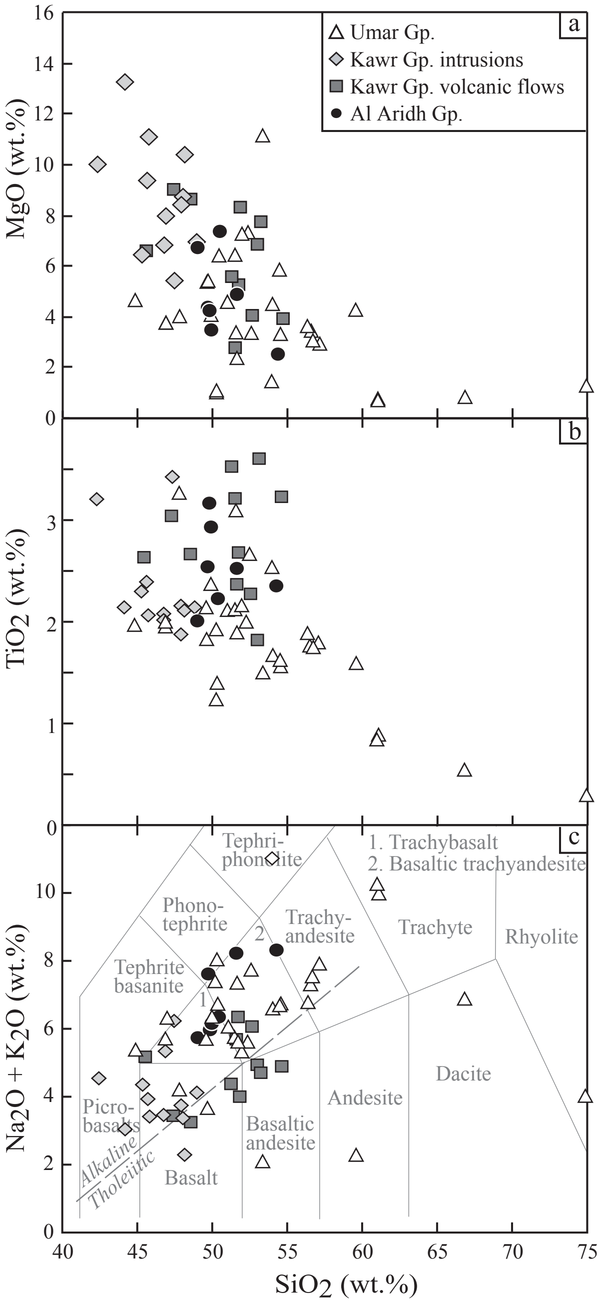

Umar Gp.
Kawr Gp. intrusions
Kawr Gp. volcanic flows
Al Aridh Gp.
a
b
c
MgO (wt.%)
TiO2 (wt.%)
Na2O + K2O (wt.%)
SiO2 (wt.%)
Tephri-phonolite
Phono-tephrite
Tephrite basanite
Trachy-andesite
1. Trachybasalt
2. Basaltic trachyandesite
Trachyte
Rhyolite
Dacite
Andesite
Basaltic andesite
Basalt
Picro-basalts
Alkaline
Tholeitic

Fig. 2

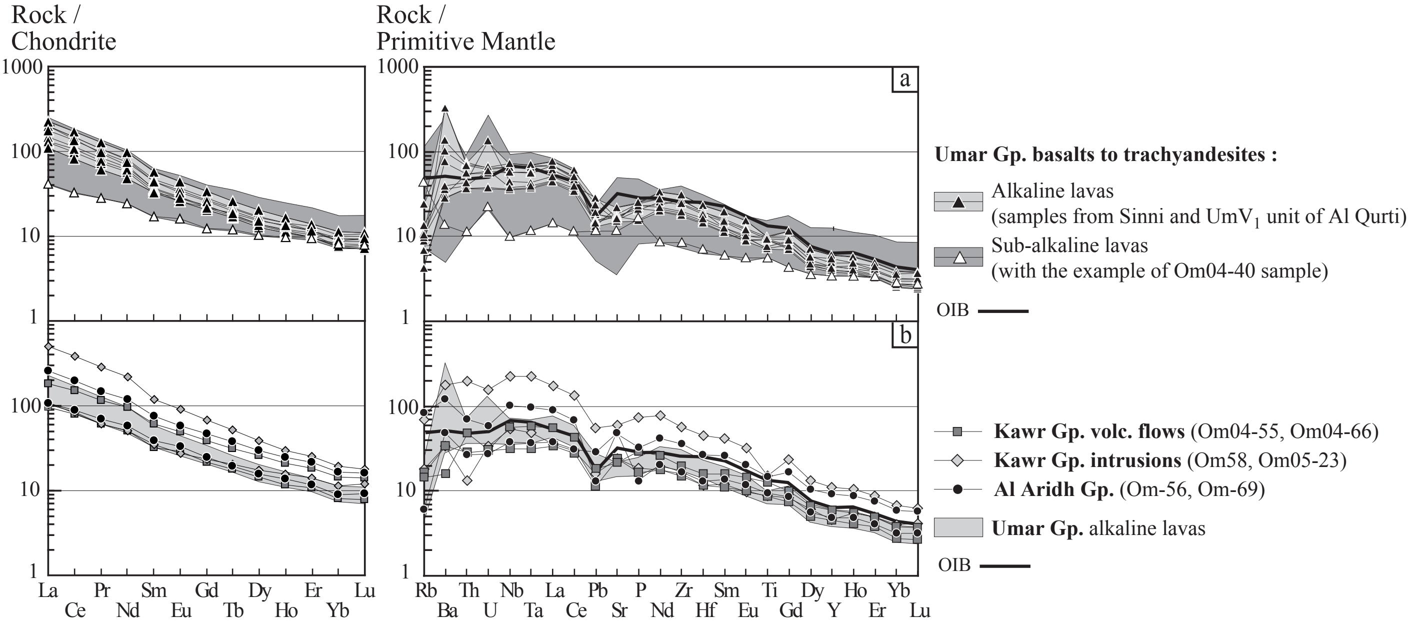

Rock /
Chondrite
Rock /
Primitive Mantle
1000
100
10
1
a
b
La
Ce
Pr
Nd
Sm
Eu
Gd
Tb
Dy
Ho
Er
Yb
Lu
Rb
Ba
Th
U
Nb
Ta
La
Ce
Pb
Sr
P
Nd
Zr
Hf
Sm
Eu
Ti
Gd
Dy
Y
Ho
Er
Yb
Lu
Umar Gp. basalts to trachyandesites :
Alkaline lavas
(samples from Sinni and UmV$_1$ unit of Al Qurti)
Sub-alkaline lavas
(with the example of Om04-40 sample)
OIB
Kawr Gp. volc. flows (Om04-55, Om04-66)
Kawr Gp. intrusions (Om58, Om05-23)
Al Aridh Gp. (Om-56, Om-69)
Umar Gp. alkaline lavas
OIB

Fig. 3

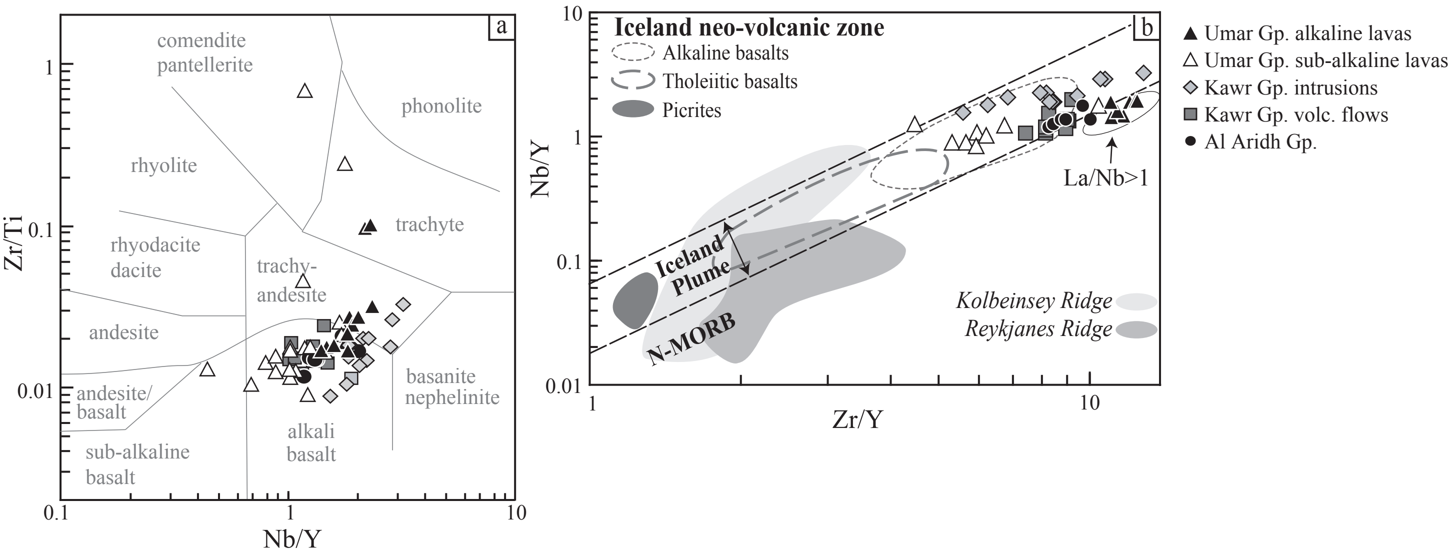

a
comendite
pantellerite
phonolite
rhyolite
trachyte
rhyodacite
dacite
trachy-
andesite
andesite
andesite/
basalt
basanite
nephelinite
alkali
basalt
sub-alkaline
basalt
Zr/Ti
Nb/Y
1
0.1
0.01
10
b
Iceland neo-volcanic zone
Alkaline basalts
Tholeiitic basalts
Picrites
La/Nb>1
Iceland
Plume
N-MORB
Kolbeinsey Ridge
Reykjanes Ridge
Nb/Y
Zr/Y
Umar Gp. alkaline lavas
Umar Gp. sub-alkaline lavas
Kawr Gp. intrusions
Kawr Gp. volc. flows
Al Aridh Gp.

Fig. 4

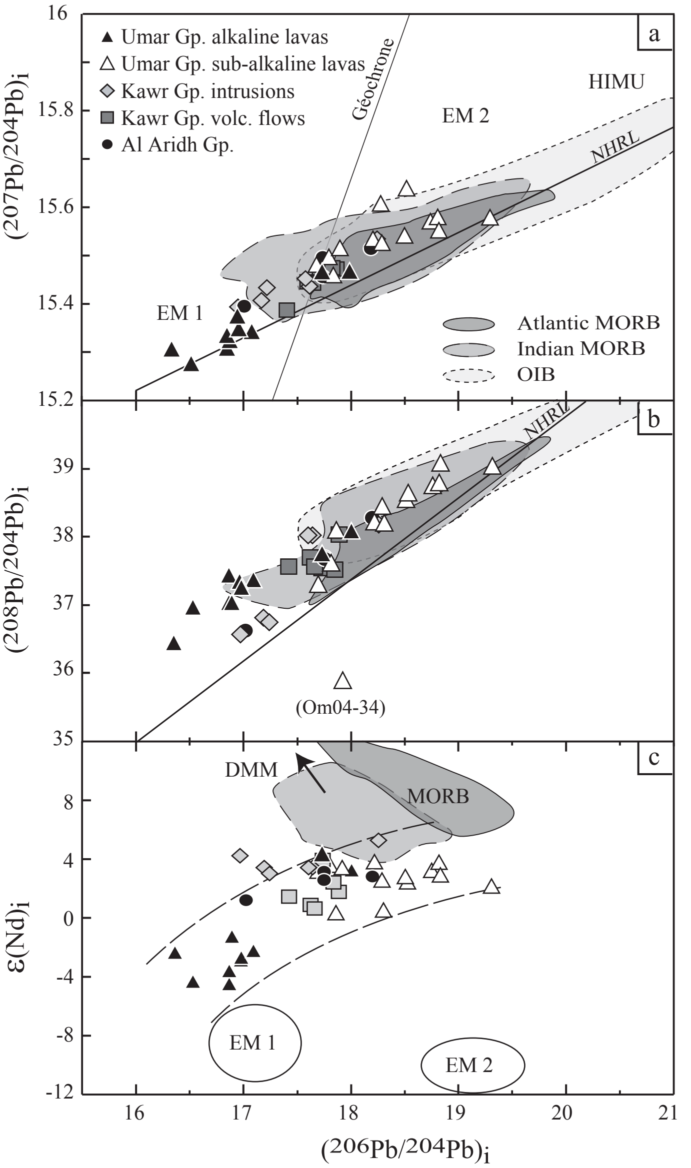

Umar Gp. alkaline lavas
Umar Gp. sub-alkaline lavas
Kawr Gp. intrusions
Kawr Gp. volc. flows
Al Aridh Gp.
Géochrone
EM 2
HIMU
NHRL
EM 1
Atlantic MORB
Indian MORB
OIB
a
b
c
(Om04-34)
DMM
MORB
EM 1
EM 2
$(^{207}Pb/^{204}Pb)_i$
$(^{208}Pb/^{204}Pb)_i$
$\varepsilon(Nd)_i$
$(^{206}Pb/^{204}Pb)_i$

Fig. 5

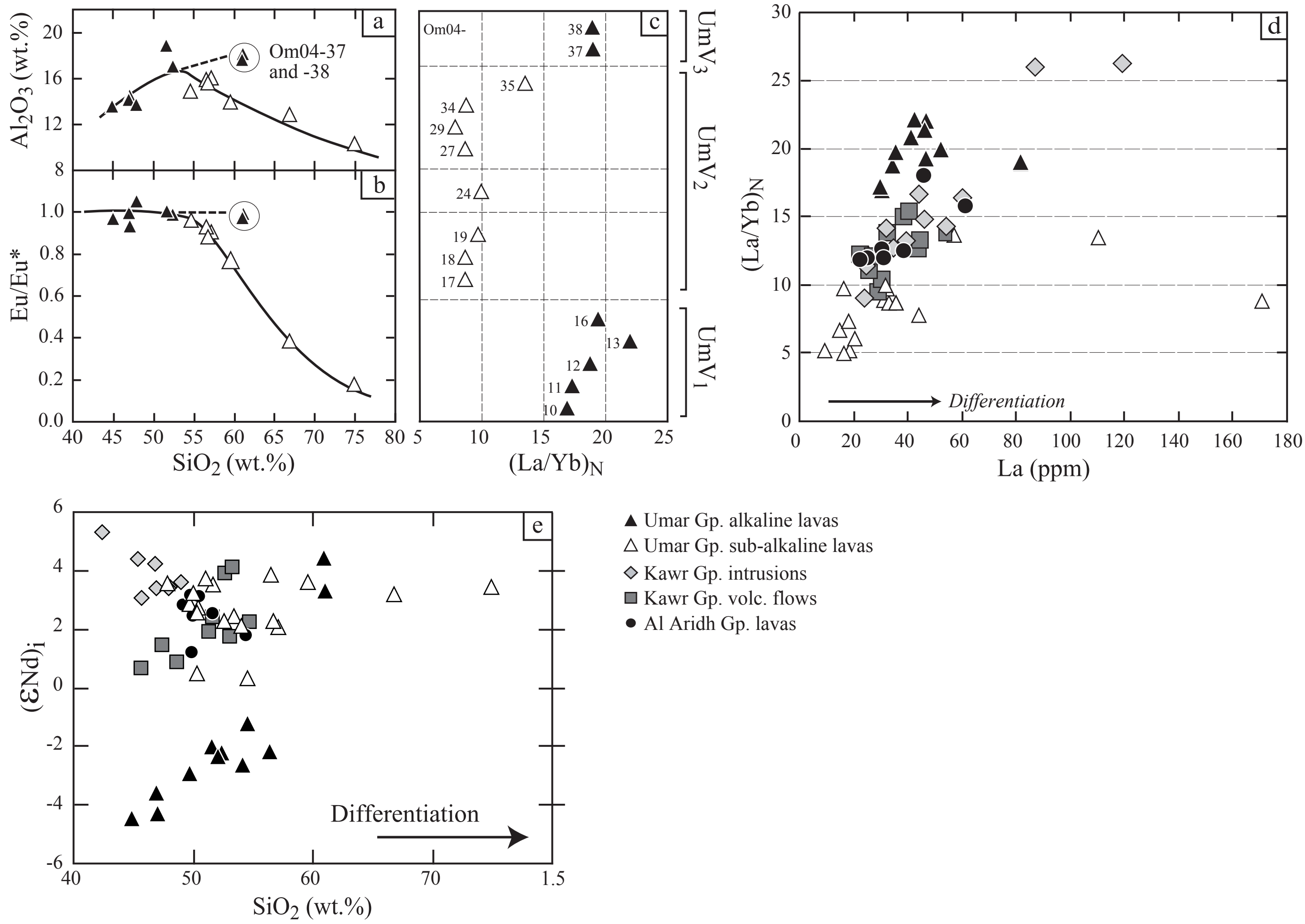

a
b
c
d
e
Om04-37
and -38
Al2O3 (wt.%)
Eu/Eu*
SiO2 (wt.%)
Om04-
(La/Yb)N
UmV3
UmV2
UmV1
La (ppm)
Differentiation
(εNd)i
Umar Gp. alkaline lavas
Umar Gp. sub-alkaline lavas
Kawr Gp. intrusions
Kawr Gp. volc. flows
Al Aridh Gp. lavas

Fig. 6

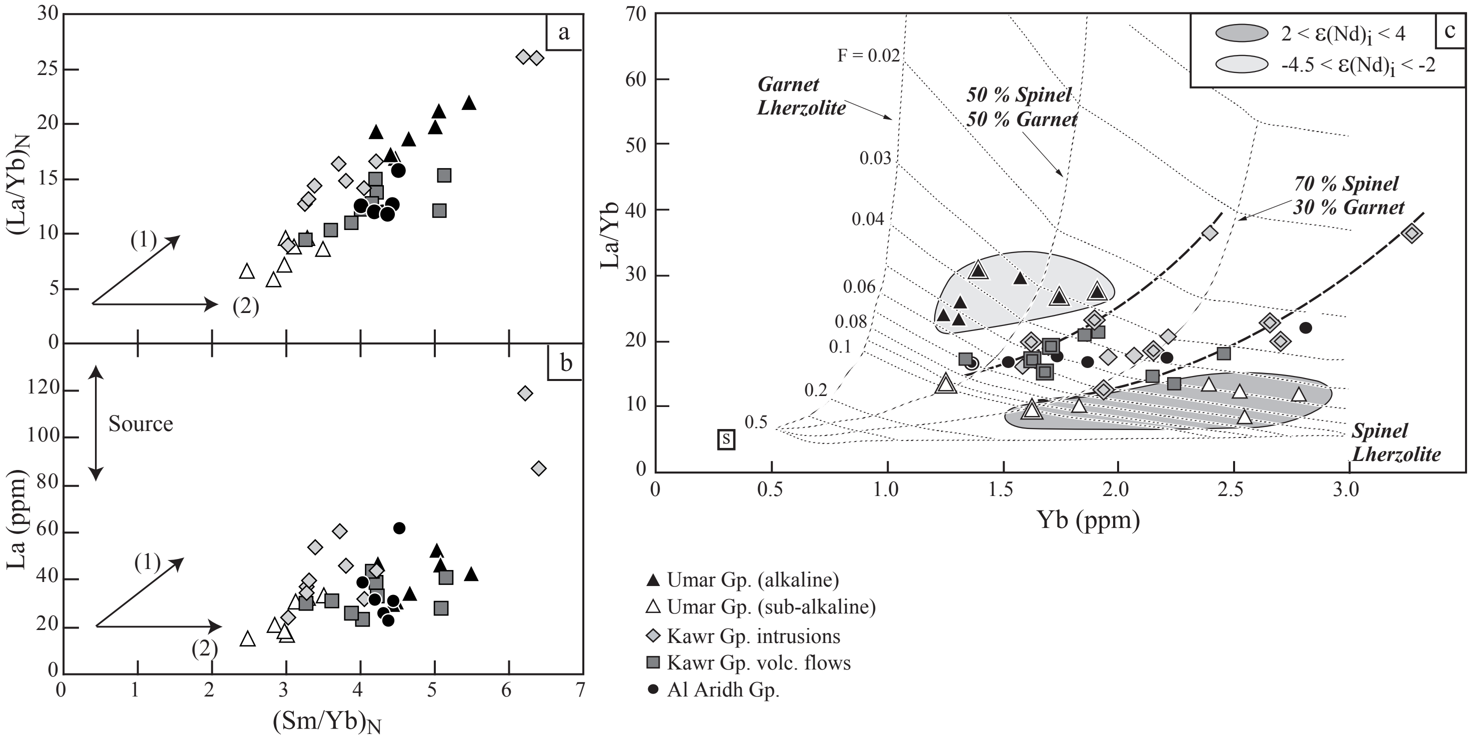

a
b
c
(La/Yb)N
La (ppm)
(Sm/Yb)N
(1)
(2)
Source
La/Yb
Yb (ppm)
2 < ε(Nd)i < 4
-4.5 < ε(Nd)i < -2
F = 0.02
0.03
0.04
0.06
0.08
0.1
0.2
0.5
Garnet Lherzolite
50 % Spinel 50 % Garnet
70 % Spinel 30 % Garnet
Spinel Lherzolite
S
Umar Gp. (alkaline)
Umar Gp. (sub-alkaline)
Kawr Gp. intrusions
Kawr Gp. volc. flows
Al Aridh Gp.

Fig. 7

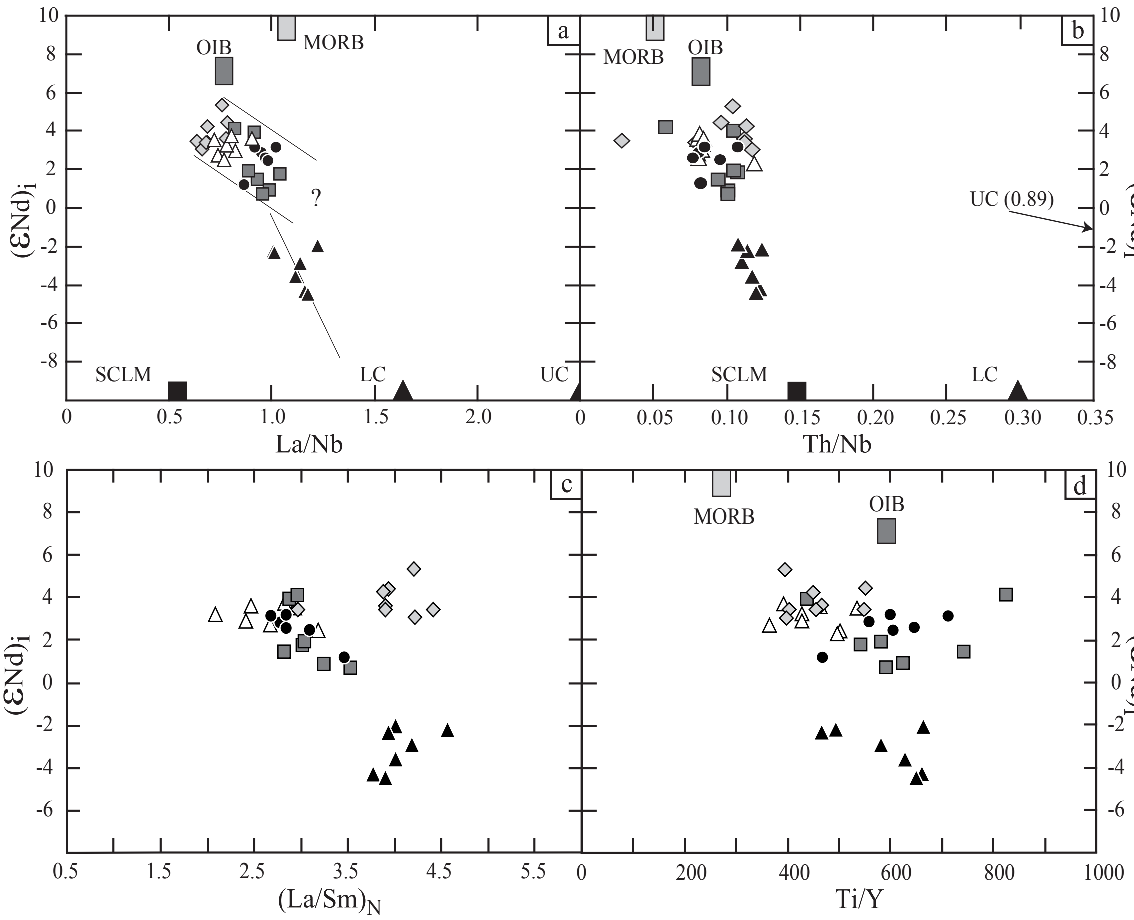

Fig. 8

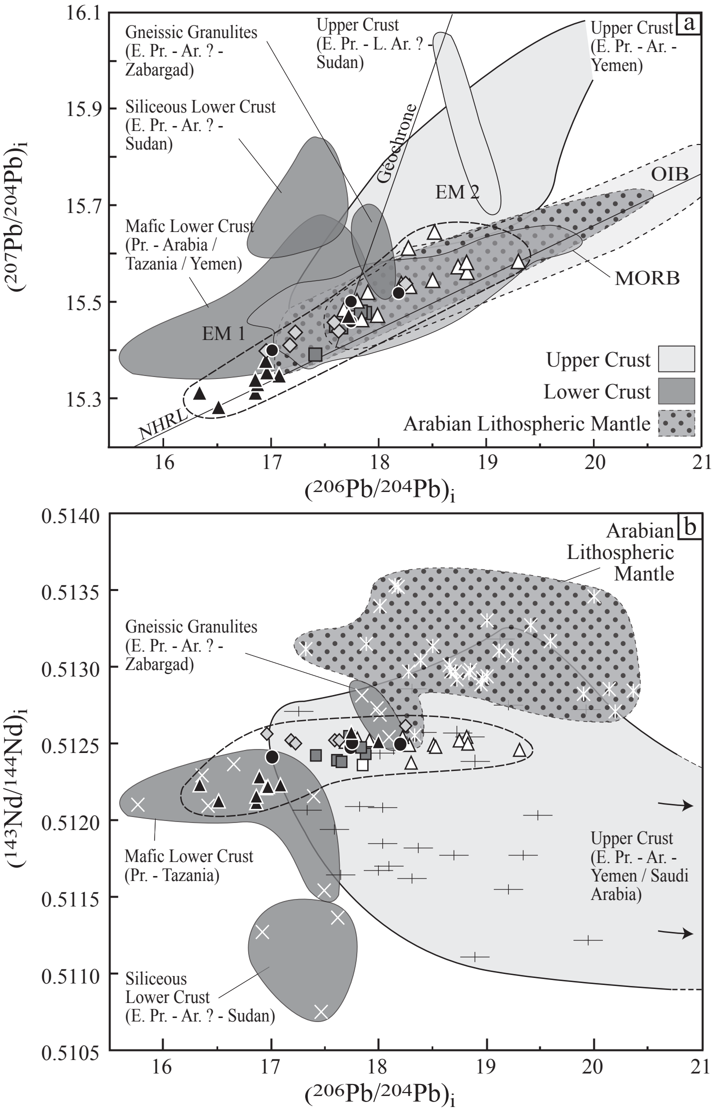

a
Gneissic Granulites
(E. Pr. - Ar. ? -
Zabargad)
Upper Crust
(E. Pr. - L. Ar. ? -
Sudan)
Upper Crust
(E. Pr. - Ar. -
Yemen)
Siliceous Lower Crust
(E. Pr. - Ar. ? -
Sudan)
Mafic Lower Crust
(Pr. - Arabia /
Tazania / Yemen)
Geochrone
EM 2
EM 1
OIB
MORB
NHRL
Upper Crust
Lower Crust
Arabian Lithospheric Mantle
$(^{207}Pb/^{204}Pb)_i$
$(^{206}Pb/^{204}Pb)_i$
b
Arabian
Lithospheric
Mantle
Gneissic Granulites
(E. Pr. - Ar. ? -
Zabargad)
Mafic Lower Crust
(Pr. - Tazania)
Upper Crust
(E. Pr. - Ar. -
Yemen / Saudi
Arabia)
Siliceous
Lower Crust
(E. Pr. - Ar. ? - Sudan)
$(^{143}Nd/^{144}Nd)_i$
$(^{206}Pb/^{204}Pb)_i$

Fig. 9

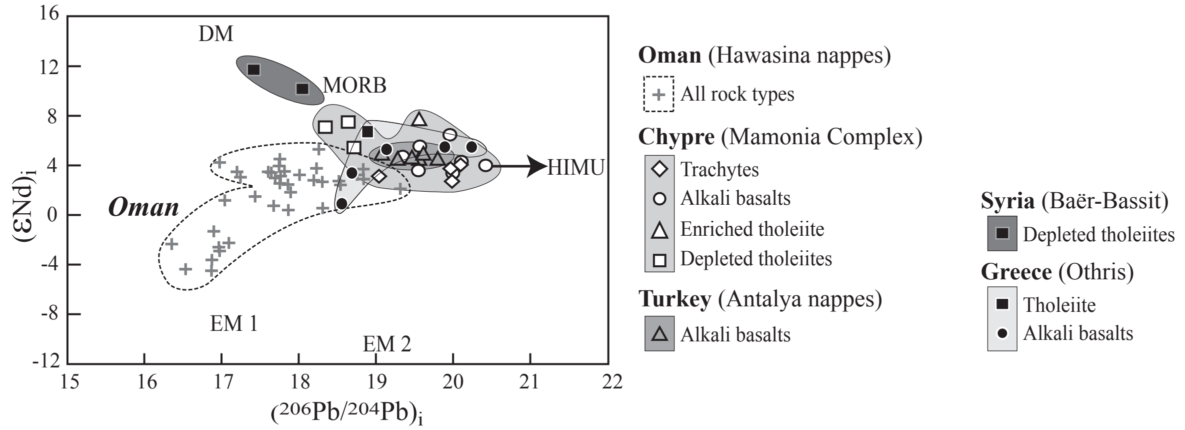

16
12
8
4
0
-4
-8
-12
15
16
17
18
19
20
21
22
(εNd)i
(206Pb/204Pb)i
DM
MORB
HIMU
Oman
EM 1
EM 2
Oman (Hawasina nappes)
All rock types
Chypre (Mamonia Complex)
Trachytes
Alkali basalts
Enriched tholeiite
Depleted tholeiites
Turkey (Antalya nappes)
Alkali basalts
Syria (Baër-Bassit)
Depleted tholeiites
Greece (Othris)
Tholeiite
Alkali basalts

Fig. 10

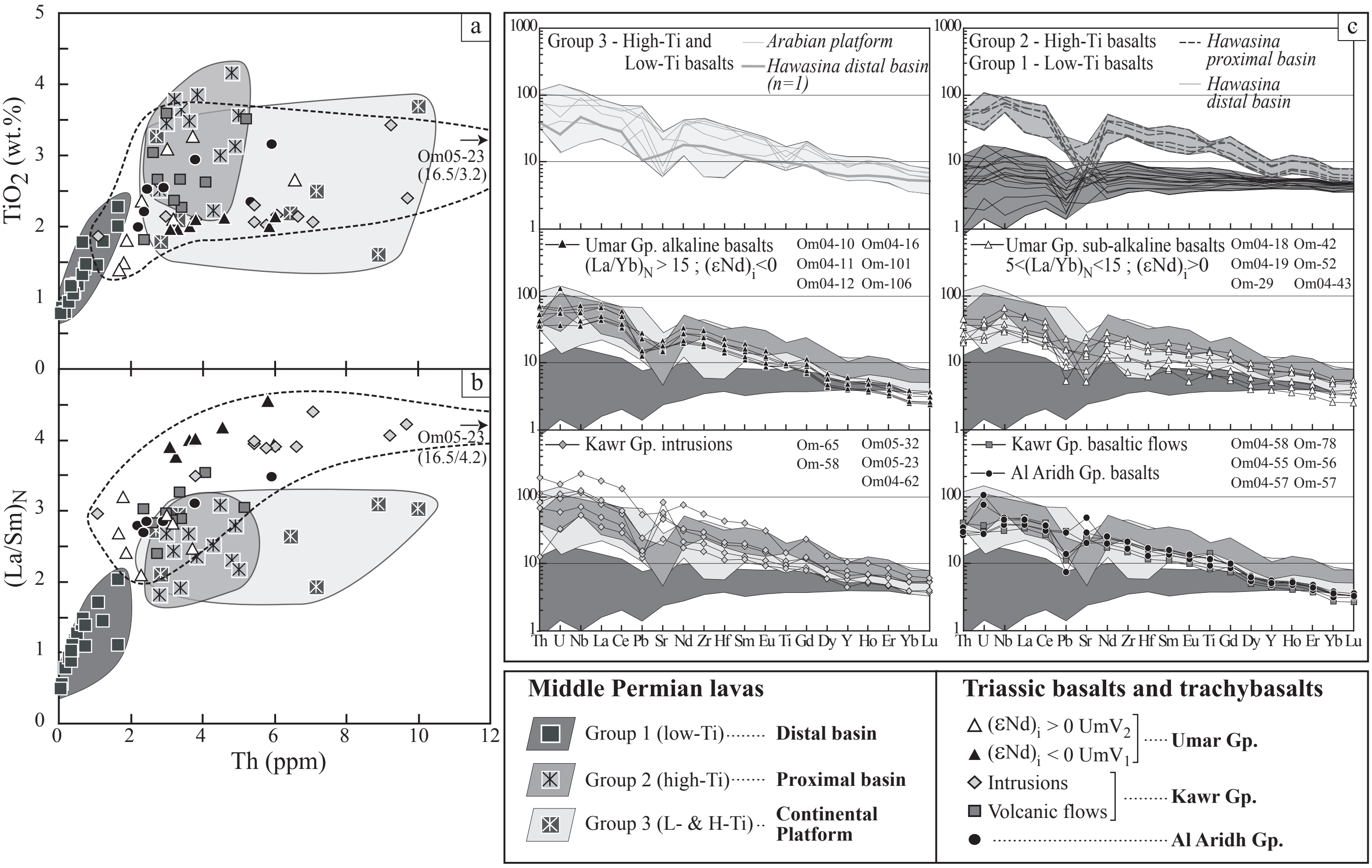

a
b
c
TiO2 (wt.%)
(La/Sm)N
Th (ppm)
Om05-23
(16.5/3.2)
Om05-23
(16.5/4.2)
Group 3 - High-Ti and
Low-Ti basalts
Arabian platform
Hawasina distal basin
(n=1)
Group 2 - High-Ti basalts
Group 1 - Low-Ti basalts
Hawasina
proximal basin
Hawasina
distal basin
Umar Gp. alkaline basalts
(La/Yb)N > 15 ; (εNd)i<0
Om04-10 Om04-16
Om04-11 Om-101
Om04-12 Om-106
Umar Gp. sub-alkaline basalts
5<(La/Yb)N<15 ; (εNd)i>0
Om04-18 Om-42
Om04-19 Om-52
Om-29 Om04-43
Kawr Gp. intrusions
Om-65 Om05-32
Om-58 Om05-23
Om04-62
Kawr Gp. basaltic flows
Al Aridh Gp. basalts
Om04-58 Om-78
Om04-55 Om-56
Om04-57 Om-57
Th U Nb La Ce Pb Sr Nd Zr Hf Sm Eu Ti Gd Dy Y Ho Er Yb Lu
Middle Permian lavas
Group 1 (low-Ti) Distal basin
Group 2 (high-Ti) Proximal basin
Group 3 (L- & H-Ti) Continental Platform
Triassic basalts and trachybasalts
(εNd)i > 0 UmV2
(εNd)i < 0 UmV1
Umar Gp.
Intrusions
Volcanic flows
Kawr Gp.
Al Aridh Gp.

Fig. 11

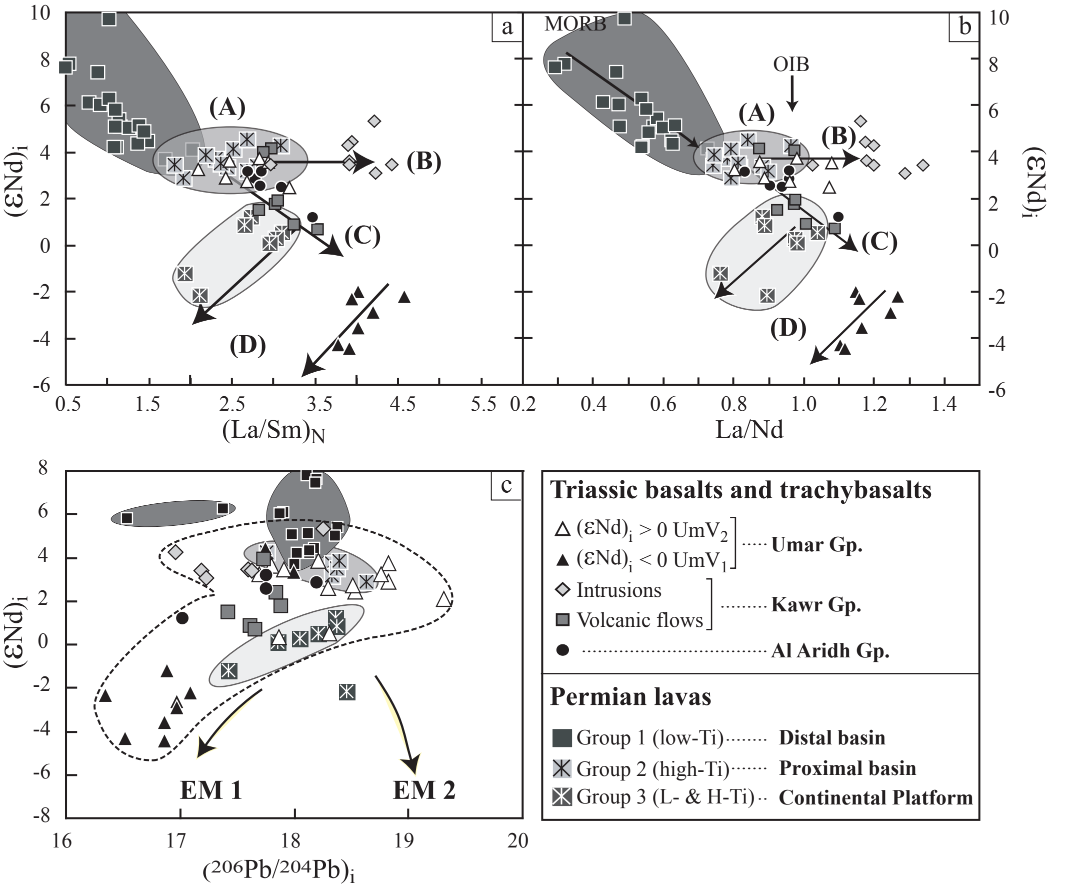

a
b
c
MORB
OIB
(A)
(B)
(C)
(D)
EM 1
EM 2
(εNd)i
(La/Sm)N
La/Nd
(206Pb/204Pb)i
Triassic basalts and trachybasalts
△ (εNd)i > 0 UmV2
▲ (εNd)i < 0 UmV1
Umar Gp.
◇ Intrusions
Volcanic flows
Kawr Gp.
Al Aridh Gp.
Permian lavas
Group 1 (low-Ti)
Distal basin
Group 2 (high-Ti)
Proximal basin
Group 3 (L- & H-Ti)
Continental Platform

Fig. 12

Table 1

Stratigraphic Gp. and position	Umar Group - Sinni Fm.									Kawr Group - Misfah Fm.			
	UmV_1 alkaline lavas					UmV_2 sub-alkaline lavas				Volcanic Flows		Intrusions	
Location	Al Qurti			Sinni		Al Qurti			Sayjah	Jabal Misfah			
Samples	Om04-11	Om04-13	Om04-16	Om-101	Om-106	Om04-24	Om04-29	Om 04-35	Om04-40	Om04-55	Om 04 57	Om- 58	Om05-23
Rock Type	TB	TA	BD	B	TB	TA	TA	R	TA	B	B	B	B
Major Elements (wt. %) recalulated on a volatile-free basis													
SiO_2	44.9	54.6	52.4	52.0	49.7	56.5	59.6	66.8	50.3	53.1	48.6	48.0	42.4
TiO_2	1.96	1.57	2.01	2.14	2.13	1.77	1.59	0.54	1.22	1.81	2.65	1.87	3.21
Al_2O_3	13.6	14.9	17.0	15.2	14.8	15.9	13.9	12.9	15.1	14.8	15.0	16.2	12.7
Fe_2O_3	9.88	5.81	9.14	9.61	8.81	8.38	12.27	6.07	7.68	11.93	9.37	12.01	15.84
MnO	0.13	0.11	0.16	0.14	0.14	0.11	0.14	0.29	0.10	0.22	0.19	0.13	0.25
MgO	4.66	3.31	7.35	7.21	5.38	3.41	4.25	0.83	1.02	6.85	8.63	8.75	10.00
CaO	19.08	12.48	5.79	7.87	12.83	5.88	5.34	5.48	16.83	6.02	11.79	9.29	9.47
Na_2O	4.95	6.41	4.36	4.47	5.43	6.67	0.35	5.30	5.96	4.36	2.83	2.66	1.39
K_2O	0.43	0.34	1.23	0.78	0.22	0.64	1.92	1.56	1.40	0.56	0.37	0.68	3.10
P_2O_5	0.45	0.50	0.55	0.53	0.53	0.70	0.67	0.22	0.35	0.35	0.52	0.40	1.58
Vol.-free total*	99.93	99.66	99.44	99.69	99.68	99.17	99.22	99.42	100.03	99.59	99.91	99.49	99.52
LOI	10.82	9.15	5.30	3.99	6.15	5.44	2.85	7.54	12.09	3.17	4.47	7.45	4.51
Trace elements (ppm)													
Sc	20	11	19	33	28	20	13	1	22	34	36	10	18
V	220	142	190	283	235	99	33	7	93	220	190	105	99
Ni	107	45	105	185	187	205	4	5	56	191	164	235	128
Co	32	18	31	46	41	29	17	3	18	44	44	59	39
Cr	*200*	*64*	*161*	*355*	*400*	*162*	*2*	*4*	*190*	*454*	*385*	*300*	*155*
Cs	0.17	0.09	0.61	0.37	0.18	0.40	0.24	0.46	1.74	0.17	0.06	0.18	0.98
Rb	6.2	4.3	15.2	6.7	2.7	11.1	29.7	18.0	27.0	10.1	2.8	11.5	43.1
Ba	198	2293	701	943	218	84	195	418	93	235	393	235	1243
Th	3.10	6.40	5.84	6.01	4.58	4.12	6.58	16.06	0.92	2.39	3.40	1.10	16.54
U	0.78	1.34	1.27	1.37	1.17	0.87	1.65	2.69	0.46	0.62	0.78	0.70	3.24
Nb	25.59	47.52	46.68	51.82	41.03	36.51	64.31	136.66	6.85	21.92	33.19	38.26	157.63
Ta	1.51	2.75	2.65	2.84	2.29	2.28	3.54	7.88	0.47	1.26	2.01	1.96	9.10
Pb	2.63	3.33	4.33	2.39	2.80	3.28	3.11	5.29	2.14	2.05	2.44	2.88	10.10
Sr	364	353	315	463	384	271	74	200	244	492	504	500	1237
Zr	200	302	295	346	273	190	437	783	93	164	232	174	630
Hf	4.43	5.94	6.05	7.20	5.92	4.34	9.37	17.12	2.15	3.55	5.04	3.56	13.60
Y	18.09	20.17	24.43	27.59	21.94	28.96	55.27	75.70	15.28	20.03	25.36	20.47	49.01
La	30.01	46.54	47.10	52.69	46.74	31.75	44.46	110.67	9.65	22.79	32.84	24.28	119.00
Ce	59.51	84.53	89.88	105.22	88.64	63.08	95.92	221.24	19.97	47.95	70.31	51.87	233.93
Pr	6.95	9.03	10.14	12.17	9.97	7.26	11.83	25.31	2.65	5.79	8.21	5.81	27.34
Nd	26.90	31.97	37.16	45.45	37.49	28.33	47.37	93.56	11.33	23.39	32.60	23.71	102.62
Sm	4.96	5.52	6.65	8.62	7.20	5.99	10.37	17.76	2.61	4.87	6.51	5.28	18.23
Eu	1.49	1.63	2.00	2.56	2.10	1.82	2.61	2.08	0.93	1.65	2.06	1.60	5.26
Gd	4.22	4.65	5.40	6.81	5.71	5.79	10.01	14.49	2.55	4.38	5.54	4.83	13.83
Tb	0.61	0.66	0.79	0.96	0.80	0.93	1.63	2.31	0.44	0.66	0.83	0.77	1.93
Dy	3.23	3.48	4.23	5.15	4.32	5.34	9.09	12.77	2.61	3.61	4.56	4.41	9.70
Ho	0.61	0.67	0.80	0.94	0.80	1.04	1.79	2.46	0.55	0.66	0.85	0.89	1.68
Er	1.58	1.82	2.13	2.32	1.94	2.86	4.82	6.63	1.57	1.78	2.16	2.31	4.17
Yb	1.25	1.52	1.75	1.91	1.58	2.29	4.09	5.88	1.37	1.34	1.71	1.94	3.27
Lu	0.18	0.23	0.27	0.28	0.23	0.33	0.61	0.83	0.20	0.20	0.24	0.30	0.46

* : Volatile-free total (not recalculated to 100%)

Table 2

	$^{143}Nd/^{144}Nd$	$^{147}Sm/^{144}Nd$	$(^{143}Nd/^{144}Nd)i$	εNd(t)	$^{206}Pb/^{204}Pb$		$^{207}Pb/^{204}Pb$		$^{208}Pb/^{204}Pb$	
					Measured	Initial	Measured	Initial	Measured	Initial
Umar Group - Sinni Fm. - Al Qurti										
Om04-10	0.512294 ± 8	0.114	0.51212	-4.29	17.4943 ± 4	16.52	15.3298 ± 4	15.28	37.8082 ± 1.2	36.96
Om04-11	0.512282 ± 15	0.112	0.51211	-4.45	17.5206 ± 5	16.86	15.3451 ± 6	15.31	37.9099 ± 1.5	37.05
Om04-11 dup.	*0.512317 ± 8*		*0.51215*			*16.86*		*15.31*		*37.05*
Om04-12	0.512329 ± 8	0.113	0.51216	-3.58	18.0601 ± 5	16.86	15.3981 ± 7	15.34	37.9644 ± 1.7	37.45
Om04-13	0.512437 ± 9	0.104	0.51228	-1.21	17.7923 ± 8	16.89	15.3738 ± 8	15.33	38.4578 ± 2.4	37.04
Om04-16	0.512392 ± 34	0.108	0.51223	-2.20	17.7423 ± 6	17.08	15.3805 ± 5	15.35	38.3722 ± 1.4	37.38
Om04-17	0.512644 ± 6	0.130	0.51245	2.08						
Om04-18	0.512734 ± 8	0.138	0.51253	3.59						
Om04-19	0.512739 ± 5	0.143	0.51252	3.54						
Om04-24	0.512732 ± 8	0.128	0.51254	3.86	18.8267 ± 7	18.21	15.5678 ± 7	15.54	39.1755 ± 2.2	38.23
Om04-27	0.512651 ± 6	0.127	0.51246	2.30						
Om04-29	0.512726 ± 5	0.132	0.51253	3.61	19.0324 ± 6	17.80	15.5617 ± 5	15.50	39.2381 ± 1.5	37.63
Om04-34	0.512692 ± 8	0.115	0.51252	3.45	18.7785 ± 15	17.91	15.5614 ± 13	15.52	41.0226 ± 3.8	35.91
Om04-35	0.512679 ± 6	0.115	0.51251	3.21	18.8748 ± 7	17.69	15.5437 ± 12	15.48	39.6130 ± 1.8	37.30
Om04-37	0.512668 ± 9	0.103	0.51251	3.34	18.7146 ± 6	18.00	15.5079 ± 6	15.47	38.9815 ± 1.6	38.10
Om04-37 dup.	*0.512644 ± 8*		*0.51249*							
Om04-38	0.512726 ± 4	0.104	0.51257	4.44	19.0516 ± 9	17.74	15.5368 ± 7	15.47	39.2490 ± 2.9	37.71
Umar Group - Sinni Fm. - Sayjah										
Om04-40	0.512578 ± 9	0.139	0.51237	0.52	18.7916 ± 8	18.30	15.5522 ± 11	15.53	38.5080 ± 3.1	38.19
Om04-42	0.512671 ± 9	0.130	0.51247	2.59	18.9639 ± 6	18.29	15.6414 ± 7	15.61	39.0166 ± 2.5	38.42
Om04-43	0.512665 ± 9	0.131	0.51247	2.45	18.8248 ± 7	18.53	15.6553 ± 7	15.64	38.9572 ± 1.9	38.63
Umar Group - Sinni Fm. - Aqil										
Om-42	0.512705 ± 10	0.143	0.51249	2.88	19.5056 ± 38	18.83	15.5908 ± 83	15.56	40.0108 ± 8.3	39.09
Om-45	0.512737 ± 12	0.135	0.51253	3.73	19.4132 ± 5	18.82	15.6080 ± 16	15.58	39.6322 ± 1.6	38.78
Om-48	0.512621 ± 11	0.107	0.51246	2.30						
Om-49	0.512630 ± 12	0.119	0.51245	2.12	22.9014 ± 41	19.31	15.7637 ± 73	15.58	40.5965 ± 7.3	39.03
Om-52	0.512693 ± 13	0.140	0.51248	2.74	19.1322 ± 11	18.51	15.5731 ± 25	15.54	38.9681 ± 2.5	38.53
Umar Group - Sinni Fm. - Sinni										
Om-29	0.512733 ± 9	0.150	0.51251	3.23	19.6348 ± 11	18.76	15.6148 ± 33	15.57	39.6663 ± 3.3	38.74
Om-97	0.512560 ± 10	0.133	0.51236	0.34	18.4306 ± 11	17.86	15.4878 ± 38	15.46	39.0129 ± 3.5	38.09
Om-99	0.512380 ± 10	0.115	0.51221	-2.63	17.7599 ± 11	16.97	15.3899 ± 43	15.35	38.2116 ± 4.3	37.25
Om-100	0.512406 ± 10	0.111	0.51224	-2.02						
Om-101	0.512395 ± 8	0.115	0.51222	-2.33	17.6334 ± 7	16.35	15.3730 ± 22	15.31	38.2907 ± 2.2	36.45
Om-106	0.512368 ± 7	0.116	0.51219	-2.90	17.9091 ± 6	16.97	15.4220 ± 20	15.37	38.5366 ± 2	37.33
Om-107	0.512397 ± 8	0.110	0.51223	-2.15						
Kawr Group - Misfah Fm. - Jabal Misfah volcanic flows										
Om04-52	0.512740 ± 3	0.131	0.51254	3.92	18.4416 ± 16	17.73	15.5010 ± 5	15.46	38.6140 ± 0.6	37.54
Om04-55	0.512621 ± 4	0.126	0.51243	1.75	18.5782 ± 8	17.88	15.5096 ± 9	15.47	38.9022 ± 1.7	38.03
Om04-56	0.512652 ± 4	0.125	0.51246	2.40	18.3903 ± 18	17.85	15.5036 ± 5	15.48	38.7267 ± 0.6	37.51
Om04-57	0.512569 ± 2	0.121	0.51239	0.88	18.3430 ± 7	17.62	15.4823 ± 11	15.45	38.7372 ± 0.6	37.70
Om04-58	0.512609 ± 4	0.128	0.51242	1.46	18.0598 ± 9	17.42	15.4213 ± 7	15.39	38.4593 ± 2	37.55
Om04-58 dup.					*18.0597 ± 11*		*15.4220 ± 11*		*38.4589 ± 2.8*	
Om04-63	0.512558 ± 6	0.120	0.51238	0.67	18.1177 ± 15	17.66	15.4658 ± 5	15.44	38.4996 ± 0.6	37.56
Om04-63 dup.	*0.512568 ± 4*		*0.51239*		*18.1186 ± 16*		*15.4666 ± 5*		*38.5041 ± 0.5*	
Om04-66	0.512629 ± 3	0.125	0.51244	1.92						
Om-207	0.512649 ± 7	0.127	0.51246	2.26						
Om-66	0.512725 ± 12	0.114	0.51255	4.11						
Kawr Group - Misfah Fm. - Jabal Misfah intrusions										
Om-58	0.512721 ± 15	0.135	0.51252	3.44	18.1451 ± 7	17.60	15.4832 ± 17	15.46	38.3142 ± 1.7	38.03
Om-61	0.512705 ± 9	0.118	0.51253	3.63						
Om-62	0.512743 ± 10	0.116	0.51257	4.42						
Om-65	0.512696 ± 10	0.119	0.51252	3.43	18.8151 ± 6	17.63	15.4988 ± 15	15.44	39.2059 ± 1.5	38.03
Om04-61	0.512698 ± 6	0.120	0.51252	3.43	18.0065 ± 14	17.18	15.4503 ± 5	15.41	38.1773 ± 0.4	36.82
Om04-62	0.512742 ± 7	0.120	0.51256	4.27	18.0312 ± 16	16.96	15.4503 ± 6	15.40	38.1788 ± 0.7	36.56
Om05-23	0.512776 ± 3	0.107	0.51261	5.32	19.0003 ± 11	18.25	15.5746 ± 3	15.54	39.4324 ± 0.4	38.19
Om05-32	0.512678 ± 5	0.119	0.51250	3.06	19.2816 ± 16	17.23	15.5398 ± 5	15.43	40.0011 ± 0.6	36.74
Al Aridh Group - Sayfam Fm. - Jabal Buwaydah										
Om-56	0.512689 ± 10	0.134	0.51249	2.82	18.4473 ± 7	18.20	15.5283 ± 18	15.52	38.5951 ± 1.8	38.28
Om-56 dup.	*0.512703 ± 11*		*0.51250*							
Om-57	0.512659 ± 15	0.124	0.51247	2.54	19.7132 ± 9	17.75	15.5563 ± 20	15.46	38.4000 ± 2	37.67
Om-67	0.512597 ± 12	0.109	0.51243	1.79						
Om-69	0.512589 ± 10	0.124	0.51240	1.19	18.1816 ± 7	17.02	15.4554 ± 23	15.40	38.4655 ± 2.3	36.61
Om-75	0.512645 ± 12	0.118	0.51247	2.45						
Om-78	0.512701 ± 9	0.131	0.51250	3.15	20.4541 ± 10	17.76	15.6349 ± 38	15.50	39.3558 ± 3.8	37.69
Om-80	0.512685 ± 8	0.121	0.51250	3.14						